HYDROXYAPATITE COATING ON Ti AND Ti6Al4V SUBSTRATES BY USING ELECTROPHORETIC DEPOSITION METHOD

ÖNDER ALBAYRAK

BOĞAZİÇİ UNIVERSITY
2008

HYDROXYAPATITE COATING ON Ti AND Ti6Al4V SUBSTRATES BY USING ELECTROPHORETIC DEPOSITION METHOD

by

Önder Albayrak

B.S., Mechanical Engineering, Gaziantep University, 1998

M.S., Mechanical Engineering, Mersin University, 2001

Submitted to the Institute for Graduate Studies in
Science and Engineering in partial fulfillment of
the requirements for the degree of
Doctor of Philosophy

Graduate Program in Mechanical Engineering

Boğaziçi University

2008

Dedicated to my dear mother Sıdıka and dear father Burhan.

ACKNOWLEDGEMENTS

I would like to express my sincere gratitude to my thesis supervisor Prof. Dr. Sabri ALTINTAŞ for his invaluable guidance and help during the preparation of this dissertation. I would like to mention his patience, giving me inspiration and motivation.

I am also grateful to Prof. Dr. Mahmut Ahsen SAVAŞ and Prof. Dr. Gökhan BAYKAL for their supporting guidance and positive motivation all the time.

I am very much indebted to my friends Nazım MAHMUTYAZICIOĞLU and Mehmet İPEKOĞLU, the academic staff of Mechanical Engineering Department of Boğaziçi University, to Assoc. Prof. Dr. Mehmet Ali GÜLGÜN and his assistants Çınar ÖNCEL and Osman EL-ATWANİ from the Department of Materials Science and Engineering of Sabancı University, to Prof. Dr. Cüneyt TAŞ from the Biomedical Engineering Department of Yeditepe University, and Prof. Dr. Nurfer GÜNGÖR from the Department of Physics of İstanbul Technical University for their support and help.

I also would like to thank to all my friends very much for being with me not only throughout this thesis but throughout my life.

Finally, all my sincere thanks and all my love goes to my parents. I am very much grateful to my dear wife for her patience and support.

This work was supported in part by the Turkish State Planning Agency (DPT-03K120250), Scientific and Technological Research Council of Turkey (TUBITAK-107M556) and Boğaziçi University Scientific Research Projects (BAP-05A601D and BAP-07A602).

ABSTRACT

HYDROXYAPATITE COATING ON Ti AND Ti6Al4V SUBSTRATES BY USING ELECTROPHORETIC DEPOSITION METHOD

Electrophoretic deposition method was used to coat hydroxyapatite (HA) on titanium (Ti) and its alloy (Ti6Al4V). Main focus was elimination or decreasing the crack occurrence and increasing adhesion strength. For this purpose, chemically synthesized nano sized and naturally derived submicron sized HA powders were produced. First, these powders both in calcined and uncalcined states were deposited on Ti and Ti6Al4V substrates under different coating voltages to investigate the effect of calcination and coating voltage on coating quality. The cracks became less pronounced with decreasing applied voltage. Coatings obtained using calcined powders were seen to be free of cracks before and after sintering. Further studies were conducted to increase the adhesion strength by depositing nano-sized titanium dioxide (TiO_2) powders using different coating voltages, as an inner layer between Ti6Al4V substrate and HA coating. Adhesion strength of the overall coating was found to increase with decreasing voltage used in TiO_2 deposition. Furthermore, use of the TiO_2 inner layer prevented HA decomposition. Finally, studies were conducted to create coating surface consisting of calcium phosphate (Ca-P) based bioceramics and TiO_2. This surface was expected to combine the advantages of Ca-P (osseointegration) and TiO_2 (photocatalytic bactericidal effect). TiO_2 was allowed to grow from the titanium substrate to fill in the cracks in the Ca-P coating at sintering stage, and coalescence of Ca-P/TiO_2 was observed.

ÖZET

ELEKTROFOREZ YÖNTEMİ İLE Tİ VE Ti6Al4V ÜZERİNE HİDROKSİAPATİT KAPLANMASI

Titanyum (Ti) ve titanyum alaşımı (Ti6Al4V) anayapılar üzerine hidroksiapatit (HA) kaplanmasında elekroforez yöntemi kullanılmış; kaplama yüzeyinde meydana gelen çatlak oluşumunun azaltılması, giderilmesi ve kaplamanın bağlanma dayanımının arttırılması amaçlanmıştır. Bu kapsamda, kaplama malzemesi olarak kullanılmak üzere kimyasal sentezleme ile nano boyutta ve doğal kemikten mikron-altı boyutta HA tozları üretilmiştir. Üretilen tozlar kalsinasyon işleminden önce ve sonra kaplama malzemesi olarak kullanılmış, farklı voltajlar uygulanarak Ti ve Ti6Al4V anayapılar üzerine kaplanmış, kalsinasyonunun ve voltajın kaplama kalitesi üzerindeki etkileri incelenmiştir. Kaplama voltajının azaltılmasıyla çatlak oluşma eğiliminin düştüğü belirlenmiştir. Kalsine edilen tozlar ile yapılan kaplamalarda çatlaksız yüzey elde edilmiş, sinterleme öncesi ve sonrasında çatlak oluşmamıştır. Bağlanma dayanımının arttırılmasına yönelik yapılan çalışmada Ti6Al4V anayapı ile HA kaplama arasında nano boyutta titanyum dioksit (TiO_2) tozları farklı voltajlar kullanılarak kaplanmıştır. TiO_2 ara kaplama tabakası kullanımı ile HA bozunmasının azaldığı ve TiO_2 kaplama esnasında düşük voltaj uygulanması durumunda tüm kaplamanın bağlanma dayanımının arttığı belirlenmiştir. Son olarak, kalsiyum fosfat (Ca-P) temelli biyoseramiklerin kemikle bağlanma ve TiO_2'in ultraviyole ışık altında bakteri öldürme özelliğinin biraraya getirilmesi düşünülerek Ca-P ve TiO_2 içeren kaplama yüzeyi elde edilmesine yönelik çalışmalar yapılmıştır. Bu kapsamda, Ti anayapı üzerine çatlak içeren kaplama yüzeyi oluşturulmuş, sinterleme esnasında çatlaklarda TiO_2 büyümesi sonucunda Ca-P/TiO_2 içeren yüzey elde edilmiş, ayrıca Ca-P ile TiO_2 arasında bağlanma oluşmuştur.

TABLE OF CONTENTS

LIST OF FIGURES

LIST OF TABLES

LIST OF SYMBOLS / ABBREVIATIONS

α	Alpha
β	Beta
ε	Dielectric constant
η	Viscosity of the medium
μ	Electrophoretic mobility
σ_{UCS}	Compressive strength
ζ	Zeta potential
A	Surface area of the electrode
c	Particle concentration in the suspension
d	Distance of separation
E	Electric field or field strength
E_y	Young's modulus
M	Mass deposited in time t
q	Surface charge density
t	Deposition time
ASTM	American society for testing and materials
Ca-P	Calcium phosphate
DC	Direct current
EDX	Energy dispersive X-ray
EPD	Electrophoretic deposition
FTIR	Fourier transform infrared spectroscopy
HA	Hydroxyapatite
ICDD	International centre of diffraction data
N	Naturally derived
NA	Not available
NS	Mixture of naturally derived and chemically synthesized
PDF	Powder diffraction file

pI	Isoelectric point
S	Chemically synthesized
SEM	Scanning electron microscopy
SS	Stainless steel
TCP	Tricalcium phosphate
TEA	Triethanolamine
XRD	X-ray diffraction

1. INTRODUCTION

Calcium phosphate (Ca-P) based ceramics have proved to be attractive materials for biological applications. Among these bioceramics, particular attention has been given to hydroxyapatite (HA), $Ca_{10}(PO_4)_6(OH)_2$, and tricalcium phosphate (TCP), $Ca_3(PO_4)_2$ due to their outstanding biological responses to physiological environments. Because of its close similarity in chemical composition and high biocompatibility with natural bone, synthetic HA exhibits strong affinity to host hard tissues [1, 2]. On the other hand, TCP has been proved to be resorbable in vivo with new bone growth replacing the implanted TCP [3, 4].

HA has been widely used in medical and dental applications such as dental implants, alveolar bridge augmentation, orthopedics, maxillofacial surgery and drug delivery systems [1]. Although, numerous HA synthesis techniques have been developed it is difficult to produce high purity HA because calcium phosphates have many derivatives and the synthesis of calcium phosphates strongly depends on reaction conditions [5]. The wet chemical process, which is based on precipitation route, is the most convenient and commonly used process [5, 6]. The most widely used precipitation method for production of HA powders is the acid-base method since the reaction involves no foreign element and the only by-product is water [7, 8].

Although HA has been used for bone substitute in a granular form (as powders or pastes) or as a solid block (in sintered form) [3], application of HA in the human body has been limited due to its poor mechanical properties [9]. Unlike HA, titanium (Ti) and Ti-alloys are proven to be potentially very suitable materials for load bearing bioimplant applications [10]. The concept of coating metal implant surfaces with HA combines the mechanical benefits of metal alloys with the biocompatibility of HA. Coating biologically inert metallic implants with biologically active materials, like HA, is an attempt to accelerate bone formation on initial stages of osseointegration, thus improving implant fixation [10, 11].

Many coating techniques have been employed for the preparation of HA coatings, such as plasma spraying, dip coating, chemical solution deposition, sputter coating,

biomimetic coating and electrophoretic deposition (EPD) [9, 12, 13]. The EPD process exhibits some advantages over other alternative processes, such as simplicity in setup, low equipment cost and the capability to form complex shapes and patterns [10, 14]. A high degree of control of coating deposit morphology can be obtained by adjusting deposition conditions and the ceramic powder size and shape [12]. Besides these advantages, ceramic coatings on metallic substrates present problems such as low adhesion strength, the appearance of cracks on coating surfaces as a result of shrinkage after the process of deposit drying and sintering, and HA decomposition during sintering stage [12, 15].

For practical medical applications, such as orthopedic implants, Ca-P coatings with excellent substrate adhesion have been strongly demanded to provide long-time fixation [16]. It is also particularly important for biomaterial applications that such Ca-P coatings should not be contaminated by toxic materials [17]. In recent years, number of studies on the bactericidal activity of titanium dioxide (TiO_2) photocatalyst has been growing [18, 19].

In this study, nano sized (chemically synthesized) and submicron sized (naturally derived) HA powders were produced in order to use as coating material. EPD method was used to coat HA on Ti and Ti6Al4V substrates. Investigations were focused on decreasing or eliminating the disadvantages of EPD such as crack occurrence, HA decomposition and low adhesion strength. In addition, studies were conducted to obtain coating surface consisting of Ca-P and TiO_2.

2. LITERATURE SURVEY

2.1. Biomaterials

"During the last 90 years, man-made materials and devices have been developed to replace parts of living systems in the human body. These special materials - able to function in intimate contact with living tissue, with minimal adverse reaction or rejection by the body - are called biomaterials" [20]. "A biomaterial is a nondrug substance for inclusion in a physiological system that augments or replaces the functions of a bodily tissue or organ. Furthermore, biomaterial must be mechanically adaptable for its designated function and have the required mechanical properties for the application. It has to be biocompatible and inert; that is, it must interact with the assorted tissues and organs in a nontoxic manner and not destroy the cellular constituents of the body fluids with which it interfaces" [21].

Biomaterials are essential for life and health in certain cases. They have a generally high added value for their size, and have a significant economic and clinical impact: The worldwide market for all types of biomaterials was estimated at over $5 billion in the late 1980s, but grew to about $20 billion in 2000 [22]. Orthopedic and dental applications represent approximately 55 per cent of the total biomaterials market. Orthopedic products worldwide exceeded $13 billion in 2000, an increase of 12 per cent over 1999 revenues [23].

2.1.1. Classification of Biomaterials

Biomaterials can be classified in four categories as ceramics, metals, polymers and composites (Table 2.1).

In the scope of this PhD dissertation, Ti and Ti-alloy were used as metal substrates and were coated with bioceramics HA and TiO_2. Ti and Ti6Al4V were used as models for metal and alloy in the metal implant materials subsection, and only HA, TCP (by HA decomposition in sintering stage) and TiO_2 were mentioned in the bioceramic subsection.

Table 2.1. Materials for implantation [3, 24]

Materials	Advantages	Disadvantages	Examples
Metals			
titanium and its alloys, stainless steels, Co-Cr alloys, gold	high-impact tensile strength; high resistance to wear; ductile adsorption of high strain energy	low biocompatibility; corrosion in physiological environment; mismatch of mechanical properties with soft connective tissues; high density	orthopedic fixation; screws, pins, plates, wires; intermedullary rods, stables, nails; dental implants; artificial joints
Ceramics			
aluminum oxide, hydroxyapatite, tricalcium phosphate	good biocompatibility; corrosion resistance; inert; high compression resistance	brittle; difficult to fabricate; low mechanical reliability; lack of resilience; high density	hip prosthesis; ceramic teeth; transcutaneous devices
Polymers			
silicones, teflon, dacron, nylon	resilience; easy to fabricate; low density	low mechanical strength; time-dependent deformation and degradation	sutures, arteries, veins; maxillofacial: nose, maxilla, mandible, teeth; cement, artificial tendon, joints
Composites			
	good biocompatibility; inert; corrosion resistance; high tensile strength	lack of consistency of material fabrication	artificial heart valve (pyrolytic carbon on graphite); knee joints implants (carbon fiber-reinforced high-density polyethylene)

2.1.2. Metallic Implant Materials: Ti and Ti6Al4V

Modern surgery and dentistry need metals and alloys of extreme chemical inertness and adequate mechanical strength. Metals and alloys in use include stainless steel, CoNiCr alloy, CoCrMo alloy, commercially pure Ti and Ti6Al4V alloy (Table 2.2). Ti and Ti-alloys are prominent as dental and orthopedic materials because of their high strength-to-weight ratio, lower elastic modulus, excellent corrosion resistance and apparent biocompatibility. Commercially pure Ti is a material of choice as an implant because of its biocompatibility resulting in no allergic reaction with the surrounding tissue. The average yield strength of commercially pure Ti is approximately 485 MPa. If a higher strength of the implant is necessary, for example, in hip prostheses, Ti-alloys have to be used. The most widely used alloy, Ti6Al4V, reaches a yield strength (about 950 MPa) almost double the yield strength of commercially pure Ti [25].

Table 2.2. Selected properties of metallic biomaterials [26]

Material	Young's modulus, E (GPa)	Yield strength, σ_y (MPa)	Tensile strength, σ_{UTS} (MPa)	Fatigue limit, σ_{end} (MPa)
Stainless steel	190	221-1,213	586-1,351	241-820
Co-Cr alloys	210-253	448-1,606	655-1,896	207-950
Ti	110	485	760	300
Ti6Al4V	116	896-1,034	965-1,103	620
Cortical bone	15-30	30-70	70-150	

The physiological environment is typically modeled as a 37 °C aqueous solution, at pH 7.3, with dissolved gases (such as oxygen), electrolytes, cells, and proteins. Immersion of metals in this environment can lead to corrosion, which is deterioration and removal of the metal by chemical reactions. During the electrochemical process of corrosion, metallic biomaterials can release ions, which may reduce the biocompatibility of materials and jeopardize the fate of implants. The stable, coherent TiO_2 film that forms on Ti and its alloys gives them superior corrosion resistance compared with stainless steel and Co-Cr alloys. The oxidized surface is also believed to be responsible for Ti implants becoming osseointegrated in vivo, a process whereby bone is apposed to the implant without chronic inflammation and without an intervening fibrous capsule [26].

2.1.3. Ceramic Implant Materials

The class of ceramics used for repair and replacement of diseased and damaged parts of musculoskeletal systems are termed bioceramics [27]. According to the type of bioceramics used and their interaction with the host tissue, they can be categorized as either "bioinert" (refers to a material that retains its structure in the body after implantation and does not induce any immunologic host reactions) or "bioactive" (refers to materials that form bonds with living tissue), and the bioactive ceramics may be resorbable or non-resorbable [26, 28].

The major drawbacks to the use of ceramics as implants are their brittleness and poor tensile properties. Although they can have outstanding strength when loaded in compression, they fail at low stress when loaded in tension as shown in Table 2.3 [26].

Table 2.3. Selected properties of ceramics biomaterials [26, 29]

Ceramic	Chemical formula	Young's modulus, E (GPa)	Compressive strength, σ_{UCS} (MPa)	Comment
HA $^{\text{high sint. temp.}}$	$Ca_{10}(PO_4)_6(OH)_2$	80-110	500-1000	bioactive
HA $^{\text{low sint. temp.}}$	$Ca_{10}(PO_4)_6(OH)_2$	-	-	biodegradable
TCP	$Ca_3(PO_4)_2$	33-90	460-680	biodegradable
Alumina	Al_2O_3	380	4000	bioinert
Bone-cortical	-	15-30	100-230	
Bone-spongy	-	0.05-0.5	2-12	

Although focus is on Ca-P based ceramics and TiO_2 throughout this thesis, alumina and zirconia need also to be mentioned briefly due to their use as bioceramic materials. Among bioceramics alumina has the highest mechanical properties, but its tensile properties are still below those of metallic biomaterials. Additional advantages of alumina are its low coefficient of friction and wear rate. Because of these properties, alumina has been used as a bearing surface in joint replacements [26]. Zirconia is used as the articulating ball in total hip prosthesis. The potential advantages of zirconia in load-bearing prosthesis are its lower modulus of elasticity and higher strength [30].

2.1.3.1. Calcium Phosphate (HA and TCP). Calcium phosphate based ceramics have proved to be attractive materials for biological applications. Among these bioceramics, particular attention has been given to HA and TCP for bone replacement due to their biocompatibility [31, 32]. Both forms are very tissue compatible and are used for bone substitute [3]. HA has been widely used in biomedical applications due to its close similarity in chemical composition and high biocompatibility with natural bone tissue [1]. Clinically, HA has been used as a filler for bone defects and as an implant in load-free anatomic sites (for example, nasal septal bone and middle ear). In addition, HA has been used as a coating on metallic orthopedic and dental implants to promote their fixation in bone. In these cases, the underlying metal carries the load, whereas the surrounding bone strongly bonds to HA [26]. Compared with HA, TCP has a lower calcium-to-phosphorous ratio, which increases the degradation rate when the ceramic is placed in a biological environment [3, 33]. The progressive digestion of the granules by living tissues can promote their ingrowth and, therefore, can allow implant-tissue attachment [34]. It has

been reported that TCP is replaced by bone when it is implanted in bone marrow, and it is also absorbed when implanted subcutaneously or in soft tissue [4].

2.1.3.2. Titanium Dioxide. For biomaterial applications, it is also particularly important that such Ca-P coatings should not be contaminated by toxic materials [17]. In recent years, studies on the bactericidal activity of TiO_2 photocatalyst have been growing [18]. When exposed to light, a TiO_2 photocatalyst generates an extremely strong oxidizing power against harmful substances, such as microbes, molds and odors that come into contact, and eliminates them by decomposition into carbon dioxide, water and other small molecules [19, 35].

2.1.4. Production of Hydroxyapatite Powders

A number of ceramic and chemistry based processing routes have been developed for synthesizing HA powders, however it is difficult to produce high purity HA because calcium phosphates have many derivatives and the synthesis of calcium phosphates strongly depends on the reaction conditions [5]. Most commonly used techniques for HA formation are precipitation, solid state reaction, sol-gel methods, hydrothermal route, emulsion and microemulsion techniques, mechanochemical reaction and ultrasonically assisted reaction [5, 6]. The most convenient and commonly used one among those is the wet chemical process, which is based on precipitation route [5, 6]. The most widely used precipitation method is the acid-base method which is based on using the following reaction of calcium hydroxide, $Ca(OH)_2$, with orthophosphoric acid, H_3PO_4, [5, 8]:

$$10Ca(OH)_2 + 6H_3PO_4 \rightarrow Ca_{10}(PO_4)_6(OH)_2 + 18H_2O$$

This method is suitable for an industrial production of HA since the reaction involves no foreign element and the only by-product is water; there is no need for an additional process to eliminate by-products [5, 8, 36].

Alternatively to the synthetic processing routes HA can also be produced directly from HA containing natural sources, such as bone and teeth. For this purpose bone or teeth is deprotenized by several methods leaving HA for further use [37, 38]. The most direct

way to deprotenize HA containing materials is direct calcination method which is based on burning off the organic fraction found in bone and teeth at elevated temperatures [39, 40]. The so obtained HA can further be ground or milled to regulate the particle size.

2.1.5. Need for Hydroxyapatite Coating on Metallic Implants

For a long time the repair of wear, tear and disease on the human bone has involved the use of materials that were not originally intended for such applications. These materials often are detected as foreign bodies by the patient's immune system and sometimes interact with the body in an undesirable manner. In the recent years, there is huge development in biomaterials that are specially designed to repair and reconstruct damaged or diseased parts of the human bone. Among them, HA is the most commonly used material in biomedical applications due to its high biocompatibility and close similarity to natural bone with respect to chemical composition [1, 41, 42]. Although HA has been used for bone substitute in a granular form (as powders or pastes) or as a solid block (in sintered form), application of HA in the human body has been limited due to its poor mechanical properties. Since mechanical properties of bulk HA only allow for non- or low-load bearing applications, metallic implants are usually preferred for load bearing bioimplant cases [9, 10]. The concept of coating metal-implant surfaces with HA combines the mechanical benefits of metals with the biocompatibility of HA. Coating biologically inert metallic implants with biologically active materials, like HA, accelerates bone formation in initial stages of osseointegration, improves implant fixation, and prevents the release of metal ions from the implant into the body [43, 44].

2.2. Coating Techniques and Comparison of Deposition Processes

Many coating techniques have been employed for the preparation of HA coatings, such as plasma spraying, dip coating, sputter coating, biomimetic coating, doctor blade, and EPD. Typical thicknesses according to the coating techniques are given in Figure 2.1. In Table 2.4, advantages and disadvantages of some coating techniques are given.

The most widely used coating technique for applying HA on metal substrates is plasma spraying. Although this technique exhibits high productivity, there are some

disadvantages related to the process. This technique produces a non-uniform coating when it is applied to an irregular or a porous surface. HA coatings, which are commonly produced by plasma spraying, have been shown to exhibit clinical problems such as delamination, leading to premature wear and loosening of implants. And with plasma spraying, HA particles reach a very high temperature, which induces the decomposition of HA. Similar problems are also found with sputter coating. For dip coating and doctor blade method, binders are normally used. The residuals of the binder may remain in the ceramic coating after sintering process, which affects the purity level of the coating. Biomimetic coating method is one of the promising techniques in which a substrate is soaked in a solution that simulates the physiologic conditions, for a period of time enough to form a desirable layer of Ca-P on the substrate. However, prior to the immersion in the simulated body fluid solution, the substrate is usually treated with an alkaline solution to generate a modified surface that induces the Ca-P layer formation. Moreover, this method takes a long time. A typical biomimetic Ca-P coating normally requires an immersion period of about 14-28 days, and it cannot be applied to stainless steel substrates [12, 43-45].

Another coating system that also shows great promise is EPD. The EPD process exhibits some advantages over the other alternative processes. The time required for coating is short; the process presents high reproducibility and low cost. However, HA adhesion to the metallic substrate can be unsatisfactory, and on the coating surface some HA agglomerates, weakly adhered, can be observed. The sintering process can improve coating adhesion to the substrate, but can also promote the HA decomposition [12, 44].

EPD technique was used for coating HA on Ti and Ti6Al4V substrates in the current study, and therefore explained in more details.

2.3. Electrophoretic Deposition Method

Electrophoresis (the term derives from electro + Greek phoresis - being carried; transmission) is the process whereby suspended particles travel through a fluid in response to an applied electric field. The particles themselves carry an electric charge [47].

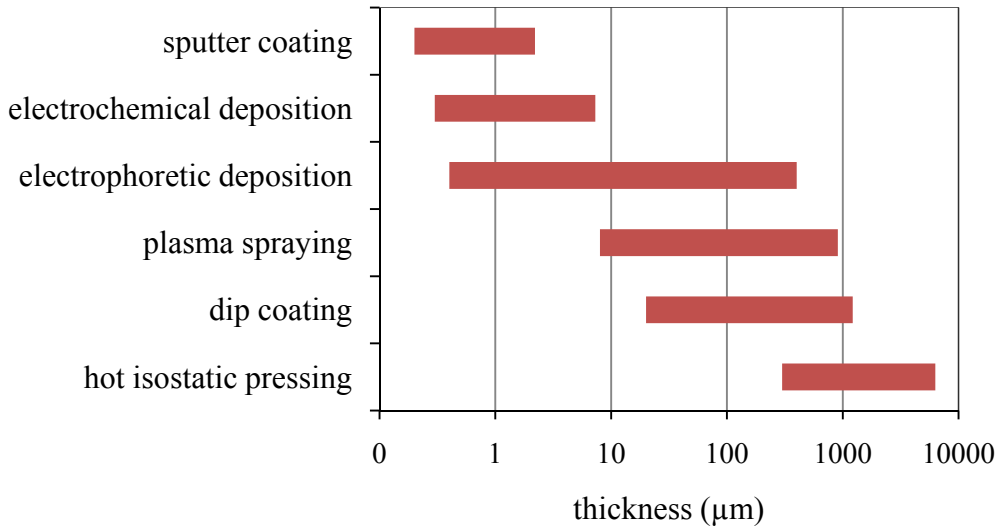

Figure 2.1. Typical thickness of coatings applied by different processes [36]

Table 2.4. Some of coating techniques and their advantages - disadvantages [46]

Technique	Advantages	Disadvantages
Electrophoretic deposition	- Uniform coating thickness - Rapid deposition rates - Can coat complex substrates - Inexpensive	- Difficult to produce crack-free coatings - Requires high sintering temperatures
Dip coating	- Inexpensive - Coatings applied quickly - Can coat complex substrates	- Requires high sintering temperatures - Thermal expansion mismatch
Sputter coating	- Uniform coating thickness on flat substrates	- Line of sight technique - Expensive - Time consuming - Cannot coat complex substrates - Produces amorphous coatings
Pulsed laser deposition	- As for sputter coating	- As for sputter coating
Hot pressing and hot isostatic pressing	- Produces dense coatings	- Cannot coat complex substrates - High temperature required - Thermal expansion mismatch - Expensive - Removal/Interaction of encapsulation material
Thermal spraying	- High deposition rates	- Line of sight technique - High temperatures induce decomposition - Rapid cooling produces amorphous coatings
Sol-gel	- Can coat complex shapes - Low processing temperatures - Relatively cheap as coatings are very thin	- Some processes require controlled atmosphere processing - Expensive raw materials

Electrophoresis involves the separation of charged species (molecules) on the basis of their movement under the influence of an applied electric field. As shown in Figure 2.2, under the influence of an applied electric field, positively charged molecules will move towards the cathode whilst negatively charged molecules move towards the anode. A molecule with no charge should remain stationary [48].

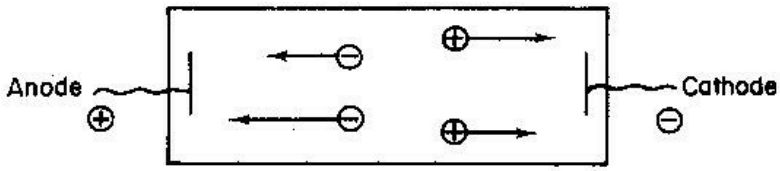

Figure 2.2. Movement of charged molecules under the influence of an applied electric field [48]

EPD is a colloidal process wherein materials are shaped directly from a stable suspension by a DC electric field. EPD is a fairly rapid low cost two-step process [49]. In a first step, particles having acquired an electric charge in the liquid in which they are suspended, are forced to move towards one of the electrodes by applying an electric field to the suspension (electrophoresis). The charged particles in suspension are moved to the substrate by the applied voltage. In a second step (deposition), these particles are deposited (discharged and flocculated) on the substrate; the particles collect at one of the electrodes and form a coherent deposit on it (Figure 2.3). The deposit takes the shape imposed by this electrode.

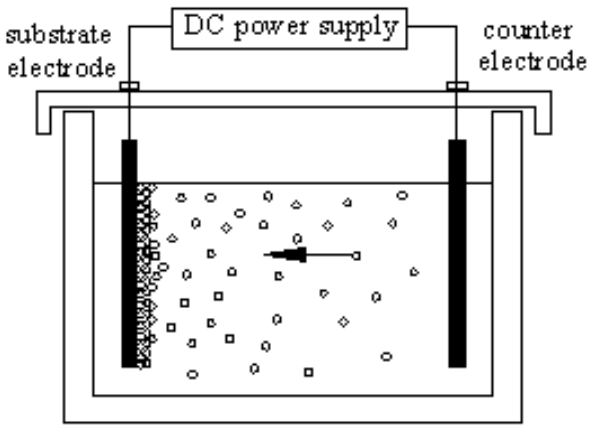

Figure 2.3. Scheme of the electrophoretic deposition method

The direction that the particles travel is dictated by their charge. Positively charged particles will migrate towards the negatively charged electrode or cathode by a process called cataphoresis. Similarly, negatively charged particles will move towards the anode via anaphoresis [50].

2.3.1. Mechanism of the Electrophoretic Deposition Method

2.3.1.1. Conditions for Electrophoretic Deposition. Electrophoresis is a phenomenon of the movement of charged particles in a colloidal suspension under the influence of an applied electric field and mobility mainly depends on the zeta potential. The stability of the colloidal particles is one of the most essential factors in considering the mechanism of the formation of electrophoretic coating [51]. Colloidal particles, which are 1 μm or less in diameter, tend to remain in suspension for long periods due to Brownian motion. Particles larger than 1 μm tend to settle and require continuous hydrodynamic agitation to remain in suspension. However, if the suspension is too stable, the repulsive forces between the particles will not be overcome by the electric field and deposition will not occur [36].

For electrophoresis to occur with larger particles, either a very strong surface charge must be obtained or the double layer region must be increased in size. This occurs at low electrolyte concentration, a condition favored in liquids of low dielectric constant. Deposition happened only when the dielectric constant of the medium was in the range of 12-25. A low dielectric constant results in low dissociation rates of the ions from the solid phase. On the contrary, a high dielectric constant decreases the double layer size and thereby reduces the electrophoretic mobility [36].

2.3.1.2. Electrophoretic Yield and Mobility. The rate of deposition can be determined approximately using Hamakers equation. Hamaker (1940) proposed that the deposited weight is proportional to the concentration of the suspension, time of deposition, surface area of the deposit, and electric field: the proportionality constant being equal to the electrophoretic mobility of the suspended particles, assuming that every particle which reached the electrode gets deposited [36, 52].

$$M = \int_0^t aAc\mu E\,dt \tag{2.1}$$

where M is the mass deposited in time t, t is the deposition time, a is the co-efficient representing the fraction of particles near the electrode that are being deposited, A is the surface area of the electrode (m^2), c is the particle concentration in the suspension (kg/m^3), μ is the electrophoretic mobility (m^2/Vs), and E is the electric field or field strength (V/m).

M, A, c, and E can be measured, and μ is determined by the properties of the suspension. The electrophoretic mobility of a molecule depends both on its net charge and on its size, which includes its shape as well as its relative molecular mass. Molecules with a high net charge will tend to move more quickly than those with a low net charge under the influence of an applied electric field. However, for molecules with the same net charge, small ones will usually move more quickly than larger ones, because the frictional forces opposing movement are greater for larger molecules [48]. The movement of ceramic particles in a nonaqueous suspension within an electric field is governed by the field strength, the pH, ionic strength and viscosity of the solution. The electrophoretic mobility of the charged particles in suspension can be presented by the Smoluchowski equation [36, 51]:

$$\mu = \frac{\zeta\varepsilon}{4\pi\eta} \tag{2.2}$$

For small particles in non-ionizing media, it is more appropriate to use the Hückel equation [36]:

$$\mu = \frac{\zeta\varepsilon}{6\pi\eta} \tag{2.3}$$

where ζ is the zeta potential, ε is the dielectric constant, and η is the viscosity of the medium. And the zeta potential can be obtained by [36]:

$$\zeta = \frac{4\pi q d}{\varepsilon} \tag{2.4}$$

where q is the surface charge density, and d is the distance of separation.

Therefore, the deposition weight of charged particles depends mainly on six parameters [36]:

- Surface properties of the colloidal particles (zeta potential),
- Electrical properties of the liquid media (relative dielectric constant),
- Colloidal suspension properties (solid content and viscosity),
- Applied voltage and time,
- Electrode area,
- Distance between the two electrodes.

However, electrophoresis is a sensitive phenomenon, which is often affected by other factors, some of which include chemical environment, particle surface topography, pH of the medium, and temperature [36].

2.3.1.3. Electric Double Layer. Most colloidal particles in aqueous solution are charged. The charge can arise from ionization of surface groups, chemical binding or physical adsorption of ions from the liquid medium. Consequently, a charged particle suspended in an electrolyte solution tends to be surrounded by an ionic cloud [53]. The distribution of the electrolyte around the surface particle is not uniform and gives rise to a structure termed the electric double layer. This configuration plays an important role in the stability of colloidal dispersions as well as their electrokinetic properties [53]. Repulsion between double layers keeps particles apart (colloidal stability) as shown in Figure 2.4 [54]. Smaller double-layers result in decreased repulsive forces that allow the particles to be attracted to each other by London Van Der Waals forces and decrease the suspension stability [55].

The electrical double layer exists at all solid-liquid interfaces, so it is generally understood that the double layer is formed at the surface of the colloidal particles [36]. The electric double layer can be regarded as consisting of two regions (Figure 2.5): an inner

region which may include adsorbed ions, and a diffuse region in which ions are distributed according to the influence of electrical forces and random thermal motion [56]. The resultant layer of ions is tightly bound and is referenced as the inner layer of the double layer. The charge density of the inner layer attracts a layer of counter ions of opposite polarity. This outer layer exists as a diffuse zone of ions sufficient in collective charge to balance the charge density of the inner layer. When the population of particles in suspension possesses similar diffuse layers flocculation is retarded and a stable dispersion prevails [57].

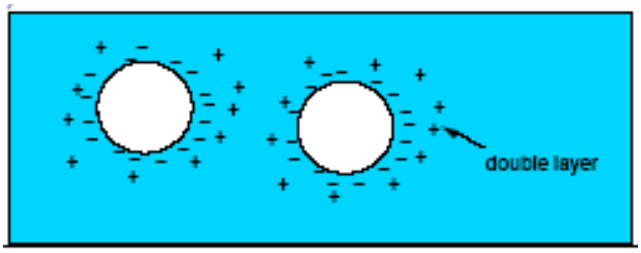

Figure 2.4. Repulsion between double layers [54]

2.3.1.4. Zeta Potential, Aggregation, and Stability of Suspension. Electrokinetic behavior depends on the potential at the surface of shear between the charged surface and the electrolyte solution. This potential is called the electrokinetic or zeta potential [56]. The zeta potential is the voltage difference between the surface of a suspended particle and the surrounding electrolyte solution. It is a measure of the effective electric charge on a colloidal particle [58].

Zeta potential is a measurement of the strength of interactions between particles in the suspension and therefore can be related to suspension stability [14]. It is a parameter to characterize colloids [51]. Zeta potential provides a measure of the level of the surface charge and serves as an indicator of the relative magnitude of the repulsion force between colloidal particles in aqueous suspension. Inter-particle repulsion counters the van der Waals attraction between colloidal particles and between particles and the walls [57].

As zeta potential relates to the particle's double layer thickness, it hence provides information on the particle agglomeration and stability of the suspension. If all of the

particles are of the same or similar material, then all of them will have the same or similar zeta potential. They will therefore repel one another with a force which depends on that potential. The particles can be prevented from aggregating with one another if the magnitude of zeta is large enough. If zeta potential becomes too small, the particles may aggregate and settle. A zeta potential of at least 25 mV (positive or negative) is normally required to achieve a reasonably stable dispersion [58]. A high absolute zeta potential value indicates the presence of a well-dispersed suspension. A higher zeta potential represents better dispersion [14].

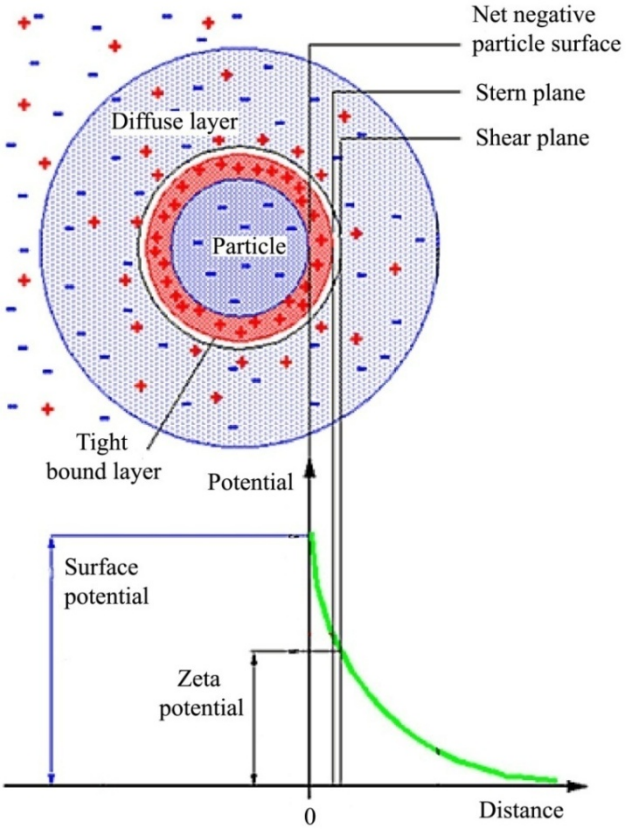

Figure 2.5. The formation of the double layer. The particle (blue) is shown to have a net negative surface charge. The particle is surrounded by a layer of ions (red) that remain tightly bound to the particle surface [57]

2.3.1.5. Suspension Preparation. Preparing a suspension from a fine powder usually requires the provision of a dispersing agent and/or the input of considerable energy, normally by stirring vigorously or by sonication [59].

The stirring process pulls the particles apart but they will only stay apart if they repel each other. This will be so if the particles have a big enough electric charge on their surface or if they become coated with the dispersing agent [59]. Normal samples can be mixed well with a high speed stirrer, until they appear to be thoroughly homogeneous. Some hydrophobic organic materials may not respond well to this treatment. High speed stirring may entrain large numbers of air bubbles to which the particles become attached. They will then float to the surface and be difficult to disperse. Therefore, the production of a vortex in the mixing process must be avoided [59].

An ultrasonic bath or an ultrasonic probe can help with the dispersion process and may be less destructive for some systems. Ultrasonication is a routine procedure for obtaining dispersion and for thoroughly redispersing a sample which may have been left standing in the lab for some time. A few minutes should normally be enough [59].

If, for some reason, the sample is too fragile to be treated so vigorously, the stirring can be replaced by a roller mixer. In that case you may have to allow several days of mixing to get the system reasonably dispersed, and it may never occur if the particles are too strongly bonded [59].

2.3.2. Process Parameters in Electrophoretic Deposition

The main factors affecting the material deposition via electrophoresis are:

- Characteristics of the environment in which the particle, molecule or ion is being studied [14, 48, 60, 61]:
  - Electrolyte concentration,
  - Particle concentration,
  - Electrical conductivity (ionic strength of the suspension),
  - pH of the medium,
  - Viscosity of the medium,
  - Temperature of the medium,
  - Electrical properties of the suspending media such as dielectric constant.

- Characteristics of the particle, molecule or ion [10, 48, 60, 61]:
  - Net charge on the molecule,
  - Particle (molecule) size,
  - Particle (molecule) shape,
  - Surface properties of the colloidal particles (zeta potential and electrical charges).

- Characteristics of the applied (electrical) field [48, 60, 61]:
  - Voltage, current (intensity and purity of current), resistance and time,
  - Surface area of the electrode,
  - Distance between electrodes,
  - Strength of the applied electric field.

The way these factors affect the EPD processes are summarized below:

Particle concentration has an effect on the viscosity on the medium. At higher concentrations, resistance arises because particles have to move out of each other's way [56].

The suspension conductivity during EPD decreases linearly with decreasing powder concentration [62].

The electrical conductivity, which is proportional to the ionic strength in the suspension, affects the deposition [14]. Ions in the suspension carry most of the current when an electric field is applied. At high ionic concentration, not only the rate of agglomeration will increase and form larger agglomerates, but the large amount of free ions in the suspension may become the main current carriers and hence reduce the speed of particle motion. Nevertheless, when the electrical conductivity is low, there will be insufficient ions to move the particles. This is because the electrophoretic motion of the particles towards an oppositely charged electrode is driven by the motion of the charges adhered onto the particles' surface. If there are only very few ionic charges available, they will not have sufficient force to move the particles [14, 51].

Conductivity increases with the increase of acidity or basicity, and it becomes very low when pH is close to the isoelectric point [51].

pH can markedly affect the net charge on a protein molecule. There is a pH value, known as the isoelectric point (pI), where the net charge on the molecule is zero. At pH values lower than their isoelectric point, these molecules will have a net positive charge; whereas at pH values above their isoelectric points they will have a net negative charge. In other words, at pH values below its isoelectric point, a particle will migrate towards the cathode during electrophoresis; whereas at pH values above its isoelectric point, it will migrate towards the anode. If pH exactly equal to its isoelectric point, the particle will have no net charge, and it should therefore not migrate during electrophoresis [56].

At any given pH, different particles will have different net charges because of their characteristic pI values. They will therefore have different migration velocities under electrophoresis [56].

pH of the suspension changes with addition of a powder. The pH of such suspensions can change substantially and unpredictably. The natural pH of a suspension tends towards the point-of-zero-charge (pI) of the powder [49].

The increase in electrolyte concentration near the depositing electrode lowers the zeta potential and induces flocculation [49].

An increase in temperature will cause the resistance to fall. An increase in temperature can change the viscosity of the medium, making it softer. The viscosity of aqueous solutions increases as their temperature decreases. This means that the frictional resistance to migration of charged molecules will increase [63]. Increase in the temperature of the bath was found to decrease the extent of microcracking, probably by increasing the density of the deposit [64].

A low dielectric constant results in low dissociation rates of the ions from the solid phase [36]. The lower the dielectric constant of the medium, the higher the electrostatic attraction between the ions and thus the higher the tendency for precipitation [64]. On the

contrary, a high dielectric constant decreases the double layer size and thereby reduces the electrophoretic mobility [36].

Particle size is an important factor for the process as the mobility of the charged particles is proportional to the size of the particles [41]. The average particle velocity increases with decreasing particle mass [56]. The rate of migration decreases for larger molecules, due to the increased frictional and electrostatic forces exerted by the surrounding medium [63].

Particles of similar size but different shapes exhibit different migration characteristics because of the differential effect of frictional and electrostatic forces [63]. For particles of equal volume the frictional coefficient increases with increasing asymmetry [56].

Zeta potential provides a measure of the level of the surface charge and serves as an indicator of the relative magnitude of the repulsion force between colloidal particles in aqueous suspension [57]. As zeta potential relates to the particle's double layer thickness, it hence provides information on the particle agglomeration and stability of the suspension. A high absolute zeta potential value indicates the presence of a well-dispersed suspension [14].

The source of electrical power used in electrophoresis is usually designed to deliver either constant voltage or constant current [48]. When constant voltage is applied, the current will increase during electrophoresis due to a decrease in resistance of the medium with the rise in temperature. Consequently, more heat will be produced resulting in more evaporation of solvent and a decrease in resistance. A constant current avoids these problems but may lead to a drop in voltage due to decreased resistance, resulting in reduced rate of migration [63]. If the current in a system is kept constant, the voltage drop across any component will be proportional to the resistance of that component [48].

At a constant voltage, the weight increment of the deposit with time declines rapidly or even stops completely because the density of electric current decreases due to increasing resistance of the system. This problem does not appear in the constant-current mode [65].

The applied voltage (or current) must be large enough to allow rapid migration of charged molecules, but not so large that excessive heat is generated [48].

2.3.3. Advantages and Disadvantages of Electrophoretic Deposition

Electrophoresis is a flexible, rapid, and low-cost process of depositing metallic and non-metallic particles on electrically conductive substrates. Like other coating techniques, it has some advantages and disadvantages:

EPD is known to be one of the most effective and efficient techniques to assemble fine particles. This technique has received keen attention due to its simplicity in setup, low equipment cost and the capability to form complex shapes and patterns [14, 41]. A short deposition time is required for electrophoretic forming or coating (a few seconds to a few minutes). The deposition rate of electrophoresis can be as high as 1 mm/min. Uniform coatings of complex shapes can be easily formed by using appropriately shaped electrodes, such as wire, coil or plate. A high degree of control of coating deposit morphology can be obtained by adjusting the deposition conditions and the ceramic powder size and shape. With increasing deposition time and voltage, thickness of the coating increases [12, 44].

Advantages of the electrophoretic deposition method can be summarized as:

- The process is simple and low cost; no expensive apparatus is required [12, 14, 41, 66, 67].
- The coating is dense and uniform; homogeneous microstructure can be obtained by this method [42, 51].
- There is capability to form complex shapes and patterns [14, 41, 68].
- Short deposition time is required for electrophoretic forming or coating (a few seconds to a few minutes) [12, 69].
- The thickness of coating is able to control by the depositing condition [36].
- There is good sinterability of the deposits [42, 51].
- There is possibility of impregnation of porous substrates [42, 51, 70].

Beside these, there are some disadvantages of HA coating on metallic substrates by electrophoretic deposition: Cracks may occur on coating surfaces after the process of deposition (during drying and sintering) [12], and also HA adhesion to the metallic substrate can be unsatisfactory, and on the coating surface some HA agglomerates can be observed. The sintering process can improve coating adhesion to the substrate, but can also promote the HA decomposition [12, 44, 46].

2.3.4. Processing and Applications of Electrophoretic Deposition

Fabrication of ceramic ware or production of a ceramic coating by electrophoresis usually follows a three-step procedure. The first step involves the preparation of a powder of the composition required in the end product, or a powder that will transform to such a composition during subsequent processing. The second step involves shaping or forming the powder into a shape similar to that required in the end product. In the final step, the formed ware is heated to high temperatures. The as-deposited coating generally has only 40 per cent of the theoretical density, so it must be sintered before being put into use. During the sintering step, the material shrinks, the porosity of the material is greatly reduced, and the mechanical strength and other required properties are developed [36].

EPD has received a great deal of attention due to its advantages for ceramic film and coatings as well as laminar ceramic composites and functionally graded materials applications. In recent years, it has also its potential in biomedical applications [51, 71]. Some applications of electrophoresis are [36]:

- Achieving strong, biocompatible material systems for many prosthetic applications involving complex loading arrangements by coating metallic prostheses with calcium phosphate ceramics.
- Obtaining plates by coating superconductive ceramics onto metal substrates.
- Forming insulating layers.
- Producing ceramic/metal coatings for thermal, mechanical, and corrosive environment.
- Producing ceramic films and composites for sensors, electronic films, and amorphous metal coatings.

2.4. Electrophoretically Deposited Hydroxyapatite Powders on Metallic Substrates

A number of reports have been published in the literature on direct EPD of oxide materials. Despite the huge amount of research effort on the process, reports on the EPD of HA as the depositing material on titanium substrates, which is one of the important areas in biomedical implant application, are limited [41]. As mentioned in Section 2.3.2, there is large number of parameters affecting EPD process. Process parameters used in some studies about HA coating on metallic substrates by EPD method are summarized and illustrated in Table 2.5.

One of the important factors for EPD is sintering. Although HA coatings can readily be deposited on metal substrates by EPD, the bonding strength between the coating and metal substrates is weak; so post-sintering is required. The sintering process can improve coating adhesion to the substrate, but can also promote the metal substrate deterioration and HA decomposition [12, 44].

Sintering of HA is complicated by the fact that HA is hydrated phase which decomposes to anhydrous calcium phosphates such as TCP at about 1200-1450 °C. At temperatures higher than 1350 °C, β-TCP irreversibly transform to α-TCP. The degradation occurs at varying degrees in the order of α-TCP > β-TCP > HA [42, 44, 66]. Decomposition of HA must be avoided since it results in enhanced in vitro dissolution and the formation of other calcium phosphate phases [72, 73].

While pure HA is chemically stable up to 1200 °C, it can decompose to TCP at a much lower temperature when heated on a metal substrate. In the presence of the underlying metal substrate, HA coatings may decompose even at a sintering temperature as low as 900 °C due to ion migration from the metal substrates into the HA coating (titanium induces the decomposition of HA above 1050 °C while for 316L stainless steel it is above 950 °C). This temperature is not high enough to ensure adequate bonding and sintering. A high temperature sintering is also unfavorable for the metal substrates since it can lead to phase transformation and grain growth. This may cause deterioration of the mechanical properties of the metal substrates. In general, commercial HA powders densify between 1100-1200 °C, but uncalcined as-precipitated (nano-particulate) HA powders densify at

Table 2.5. Process parameters used in some studies about HA coating on metallic substrates by EPD

	[12]*	**[14]***	**[15]***	**[42]***	**[51]***	**[66]***	**[74]***	**[75]***	**[76]***	**[77]***
Powder	HA	HA	HA	HA	HA	HA	HA	HA	HA	HA
Powder size	NA	0.3 μm	w: 20-30 nm l: 50-60 nm	NA	0.3 μm	average: 1.805 μm	NA	NA	NA	w: 10-30 nm l: 50-200 nm
Suspension	5 g/l (HA/ethanol)	30 g/l (HA/ethanol)	10 g/l (HA/acetic anhydride)	30 gr/l (HA/isopropyl alcohol)	20 g/l (HA/ethanol)	12.5 g/l (HA/ethanol)	15 g/l (HA/ ethanol)	5 g/l (HA/ethanol)	25 g/l (HA/ isopropyl alcohol)	(HA / n-butanol with TEA)
Voltage	50 V	NA	50 V	from 10 to 200 V	no higher than 150 V	200-400-800 V	200 V	50 V	60 V	30 V
Current density	NA	1.5 mA/cm^2	NA	current density	0.05 - 1.5 mA/cm^2	55-101-210 mA/cm^2	NA	NA	NA	NA
pH	+ charged	5 (by HNO_3)	not changed	+ charged	3-5 (by HNO_3)	NA	+ charged	+ charged	+ charged	NA
Deposition time	5 min	NA	1 min	from 10 sec to 5 min	30 sec	0.5 - 3 sec	20 sec	2 - 5 min	3 min	1 min
Substrate (working electrode)	Ti6Al4V, Ti, 316L (18×36 mm) cathode	graphite	titanium (cathode)	Ti6Al4V	carbon rod (3 mm in diameter, 4.5 cm in length)	stainless steel	Ti6Al4V (5×45×3 mm) cathode	Ti6Al4V, Ti, 316L (32×18 mm) cathode	316L (10×10×2 mm) cathode	titanium sheets (cathode)
Counter electrode	copper plate (20×35 mm) anode	stainless steel	platinum (anode)	NA	stainless steel cylinder	platinum	copper strip (10×50mm) anode	copper plate (20×35mm) anode	316L (30×90×1 mm) anode	platinum (anode)
Distance between electrodes	NA	30 mm	20 mm	15 mm	30 mm	10 mm	6 mm	NA	10 mm	7 mm

Table 2.5. Process parameters used in some studies about HA coating on metallic substrates by EPD (continue)

	[12]*	**[14]***	**[15]***	**[42]***	**[51]***	**[66]***	**[74]***	**[75]***	**[76]***	**[77]***
Deposition area	NA	1 cm^2	NA	NA	NA	1 cm^2	NA	NA	1 cm^2	1 cm^2
Drying	slowly dried in a sealed desiccator	dried in air for 24h	dried at room temperature in air	dried in air in an oven at 60°C for 2h	drying in air for 24 h	NA	dried in a fan assisted oven at 60°C for 0.5h	slowly dried in a sealed desiccator (5h)	NA	NA
Sintering	875-1000°C. heating rate: 100°C/h; cooling rate: 50°C/h; soaking time: 1 h; with argon atmosphere.	1200°C for 2h; heating rate: 1.5°C/min	850ºC for 2h; heating rate: 3ºC/min; cooling rate: 2°C/min; with argon atmosphere	930°C for 2h; vacuum sintering (1.33×10^{-4} Pa)	1150-1300°C for 2h; heating rate: 1.5°C/min; in air atmosphere	800ºC for 2h; heating rate: 100ºC/h; cooling rate: 50°C/h.	NA	875-1000°C. heating rate: 100°C/h; cooling rate: 50°C/h; soaking time: 1h; with argon atmosphere.	800°C for 1h; vacuum sintering (10^{-5} torr)	850ºC for 2h heating rate: 200ºC/h, cooling rate: 50°C/h; with argon atmosphere
Coated layer thickness	10-15 µm	NA	NA	NA	NA	NA	30 µm	NA	NA	50 µm

NA: not available
TEA: triethanolamine
* : reference number

about 1000 °C. Nanosized HA particles obtained by the wet process method enable the HA coating to achieve a high density at a relatively low sintering temperature [12, 72]. To achieve sintering at this temperature, it is required that coatings with good particle packing be formed. To obtain this type of coatings, submicron and homogeneous particles are required in suspension during the EPD process. In this way, the migration of the particles will be faster and more uniform [42, 66].

Wei et al. [74, 75] mentioned that temperatures above 900 °C can potentially have deleterious effects on titanium and stainless steel implants, principally via surface oxidation, grain growth and phase changes that spoil the mechanical properties. The mechanical properties of titanium alloys and 316L stainless steel degrade significantly when heated above 1050 °C. Therefore, densification needs to be conducted at as low a temperature as possible and in a highly oxygen depleted furnace atmosphere. In the studies reported in [74, 75], Wei et al. have stated that an oxidation layer was formed on the surface of HA coated metallic substrates at an elevated temperature, which became a potential weak layer for the bonding between HA and the metal. Elevated temperatures can also be deleterious for the HA coating.

In EPD application, the sintering process improves densification and bonding of the green coating, but also promotes HA decomposition. One way to alleviate the problem of HA decomposition at high temperatures in sintering is the usage of interlayers between substrate and HA coating. Wei et al. [12] and Wang et al. [51] used HA, Zhitomirsky and Gal-Or [42] used TiO_2 as inner layer. Wei et al. [12] observed that with the application of the dual HA coating layer, the decomposition of the second HA coating layer was significantly less than that observed in the primary coating layer. They stated that interlayers act as a diffusion barrier for ionic transport of metals ions to HA layer during sintering (reduce the decomposition of the HA powders in the second layer); and moreover the outer layer fills the cracks on the previous coating surface [12, 51]. (Reasons of crack occurrence are mentioned in the pages below).

Although cracks on surfaces were filled by outer coating layer, cracks may deteriorate adhesion strength. To improve adhesion strength, a crack-free, dense and homogeneous inner layer between HA and metal substrate can be used [78]. Nie et al. [68]

used dense TiO_2 film as the inner layer between titanium alloy substrate and HA top layer to possess a very good combination of bioactivity, chemical stability and mechanical integrity. In the study of Kumar and Wang [79], TiO_2 powders were coated on Ti6Al4V substrates as the first layer, then HA-TiO_2 composite layers of different weight ratios were coated on TiO_2 layer. However, the effects of TiO_2 layer on the adhesion strength of the overall coating were not investigated in the studies of [68] and [79]. Although Wei et al. [12] investigated the adhesion strength of HA coating, HA powders used as inner and outer layer were both the same; therefore no change occurred in the structure of coating layers; and sintering was applied after the deposition of every single layer.

Because of densification during sintering, shrinkage and cracking of the coatings can occur. Also thermal stress induced by differences in thermal expansion coefficients (Table 2.6) between metal and the ceramic film during sintering and cooling leads to cracking. This was predominantly observed with thicker coatings greater than 20 μm, obtained at higher applied potentials and time [72].

Wei et al. [12, 75] mentioned that, during the heating process, the metal substrates expanded, but the HA shrank due to densification at elevated temperatures. On the assumption that it is well bonded to the substrate, the HA coating would be subjected to a tensile stress, causing cracking of the coating. However, the bonding will not occur until elevated temperatures so the initial relative movement (substrate-coating) will not necessarily crack the coating. The other critical issue is whether the HA coating will be subjected to a compressive stress or a tensile stress on cooling. For the Ti and Ti6Al4V substrates, with thermal expansion coefficients slightly lower than that of HA, the coatings underwent a slight tensile stress during the cooling. This could exacerbate the cracks formed during the sintering shrinkage, thereby reducing the adhesive strength of the coating. Relatively low adhesive strengths were obtained for the coatings on Ti and Ti6Al4V. Conversely, stainless steel would have subjected the coating to a compressive cooling stress, thereby tending to constrain the cracks. Relatively high adhesive strengths were obtained for the coatings on stainless steel. With regard to thermal expansion, titanium places the coating in tension, stainless steel places it in compression, and therefore the coated titanium would be more susceptible to cracking. With regard to oxide scale, the

thickness of the oxide interlayer is much greater for titanium, and this layer is a potential source of weakness [12, 36, 75].

Table 2.6. Thermal expansion coefficients of some materials [12, 75, 80]

Material	Thermal expansion coefficient (α)
Ti	$10.4 \times 10^{-6} K^{-1}$
Ti6Al4V	$10.3 \times 10^{-6} K^{-1}$
Merck HA	$14.6 \times 10^{-6} K^{-1}$
316L	$20.5 \times 10^{-6} K^{-1}$
Al_2O_3	$9.0 \times 10^{-6} K^{-1}$
ZrO_2	$10.3 \times 10^{-6} K^{-1}$

From the study of Wei et al. [12] cracks on the coatings were observed for Ti, Ti6Al4V and 316L stainless steel substrates and all sintering temperatures as shown in Figure 2.6. The cross-sectional morphologies of the dual coatings on all three substrates sintered are shown in Figure 2.7. Although the sintering process was conducted in a high purity argon atmosphere, a thick, porous oxidation layer was clearly observed on the surface of Ti (about 7 μm) and Ti6Al4V (about 6 μm). In contrast, a much thinner oxidation layer (about 1 μm) was formed on the surface of the 316L stainless steel substrate during sintering. This oxidation layer was always present as an interlayer between the HA coating and the metal [12].

Zhitomisky and Gal-Or [42] have prepared two different HA powders (coded as HA-1 and HA-2) to EPD in order to investigate their effects on crack occurrence. HA-1 powder was prepared by washing the precipitate obtained with water and drying at 60 °C for 48 h. For HA-2 preparation, the precipitate obtained was washed with water and finally with isopropyl alcohol and stored in a moisture-free atmosphere for three weeks. The weight of HA-2 was controlled and no weight change was observed after this period. After milling in an agate mortar the HA-1 and HA-2 powders obtained were used for the study. Authors observed that sintered HA-2 coatings were relatively dense and adherent to the substrate. In contrast, HA-1 coatings can easily be removed from the substrates. Figure 2.8 shows HA coatings of TiAlV substrates after sintering. SEM pictures exhibit partial

densification of coatings, as indicated by a decrease of porosity, particle coalescence and interparticle neck formation. Cracks were also observed in coatings (Figure 2.8b) near coating -substrate interface [42].

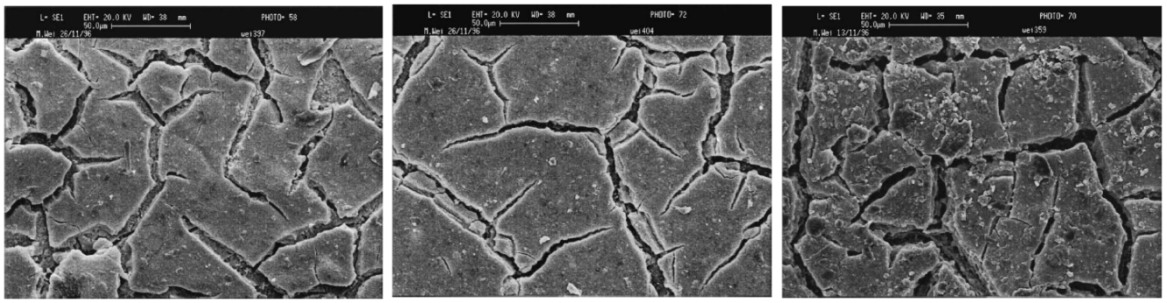

Figure 2.6. (from left to right) Surface morphologies of HA coating on Ti substrate, Ti6Al4V substrate, and 316L substrate after sintering at 925°C for 1 h [12, 75]

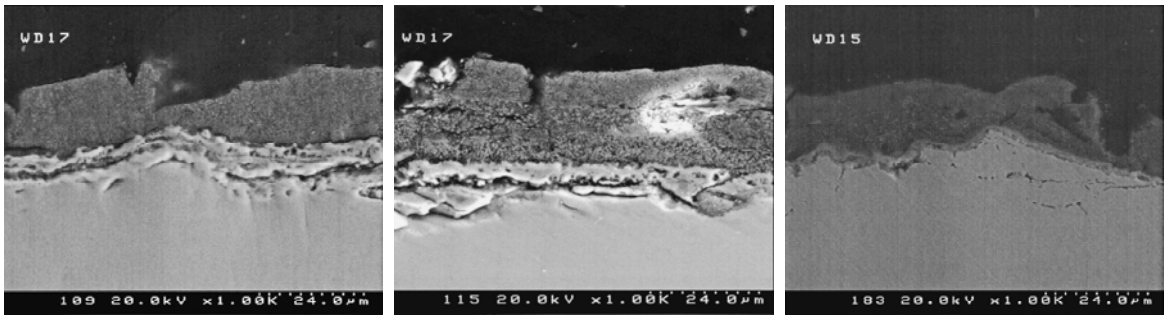

Figure 2.7. (from left to right) Cross-section morphologies of HA coating on Ti, Ti6Al4V and 316L substrates [12, 75]

Xiao and Liu [77] have used dispersant triethanolamine (TEA) in HA/n-butanol suspension. They observed that the HA coating deposited in this suspension was a crack-free and densely packed as shown in Figure 2.9.

In the study of Mondragon-Cortez and Vargas-Gutierrez [66], crack free HA coatings on 316L stainless steel were produced by EPD in ethanol at 200, 400 and 800 V during 0.5 to 3 sec. The particle size distribution of the starting suspension was 0.275 to 4.88 µm, with an average size of 1.805 µm. Coatings were obtained and then sintered at 800 °C for 2 h. The sintered coatings presented a very homogeneous polycrystalline

structure free of cracks. Obtained surface morphology by SEM before sintering (Figures 2.10 and 2.11) and after sintering (Figure 2.12) are shown below.

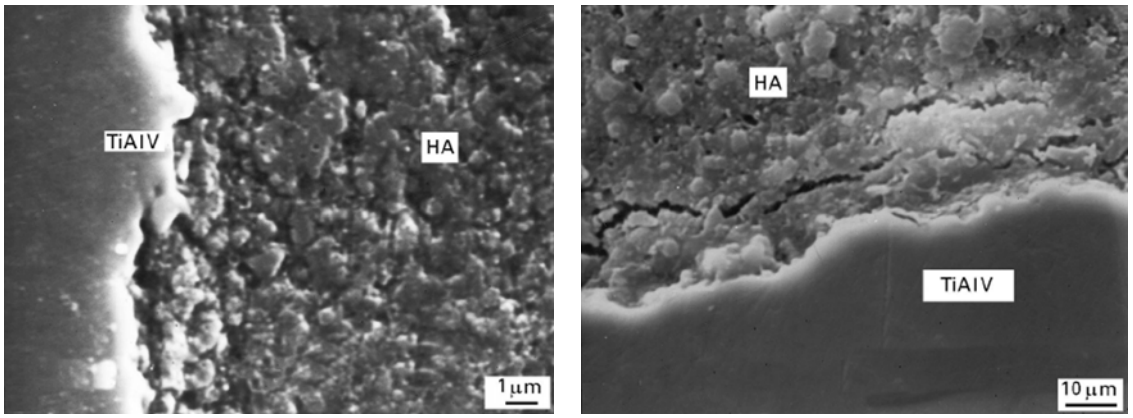

(a) (b)

Figure 2.8. SEM pictures of sintered HA coatings on TiAlV substrates:
(a) HA-1 coating, (b) HA-2 coating [42]

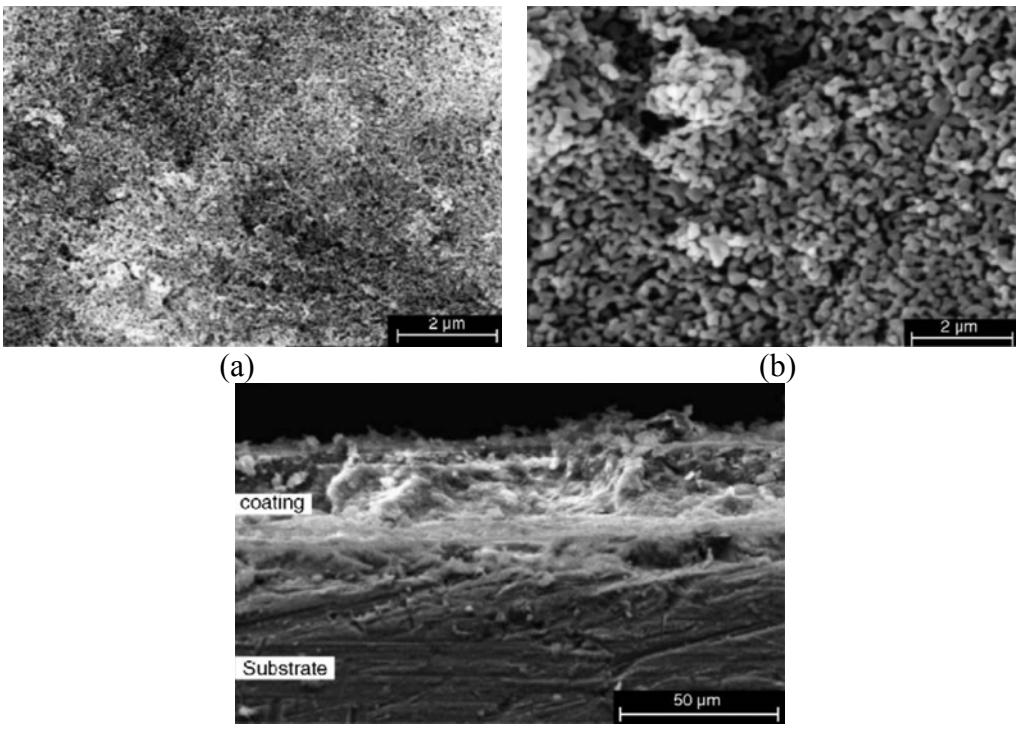

(a) (b)

(c)

Figure 2.9. SEM images of HA coatings after sintering at 850 °C for 2 h:
(a) with TEA (12 mL L^{-1}), (b) without TEA, (c) cross-section morphology [77]

In the study of Mondragon-Cortez and Vargas-Gutierrez [66], HA submicron particle coatings were obtained by EPD on metallic substrates in two different ways: at high voltage in short times and at low voltage with longer times. In the second way, the smallest particles can be deposited although longer times are required to achieve thick coatings. On the other hand, it has been found that high voltage EPD can promote agglomeration of particles, gas evolution during the assays, and corrosion effect on the metallic substrate. However, Mondragon-Cortez and Vargas-Gutierrez did not observe any of these phenomena due to the faster high voltage application. They stated that, at EPD particle size range increases with applied voltage (Figure 2.10). Mondragon-Cortez and Vargas-Gutierrez [66] expressed that the high voltage and the time of deposition were important factors in the preferential deposition of small particles. The smallest particles reached the highest electrophoretic velocity, and therefore these were the first ones in being deposited. Figure 2.11 shows different particle size deposited during 0.5, 2, and 3 sec at 800 V.

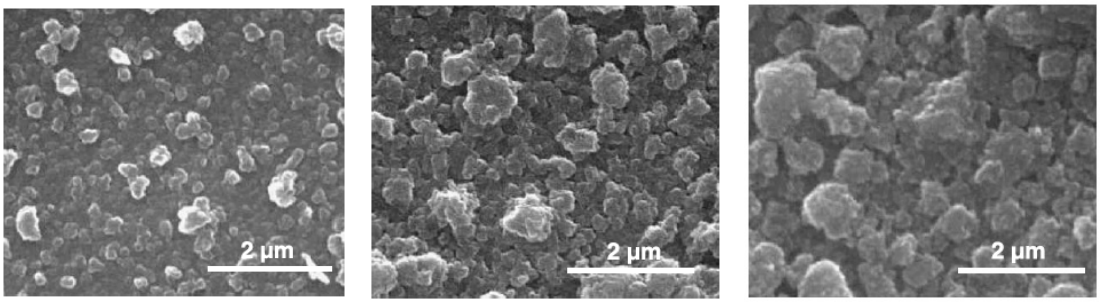

Figure 2.10. Surface morphology by SEM of coatings obtained during 1 sec at different applied voltage: 200 V, 400 V and 800 V (from left to right) [66]

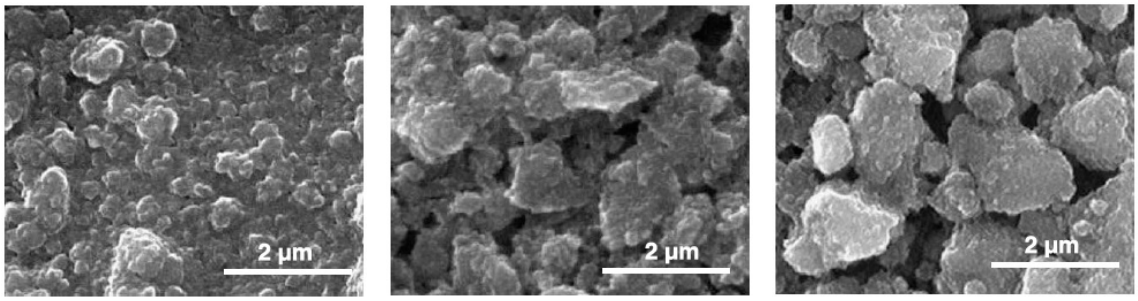

Figure 2.11. Surface morphology by SEM of coatings obtained at 800 V during different applied time: 0.5 sec, 2 sec and 3 sec (from left to right) [66]

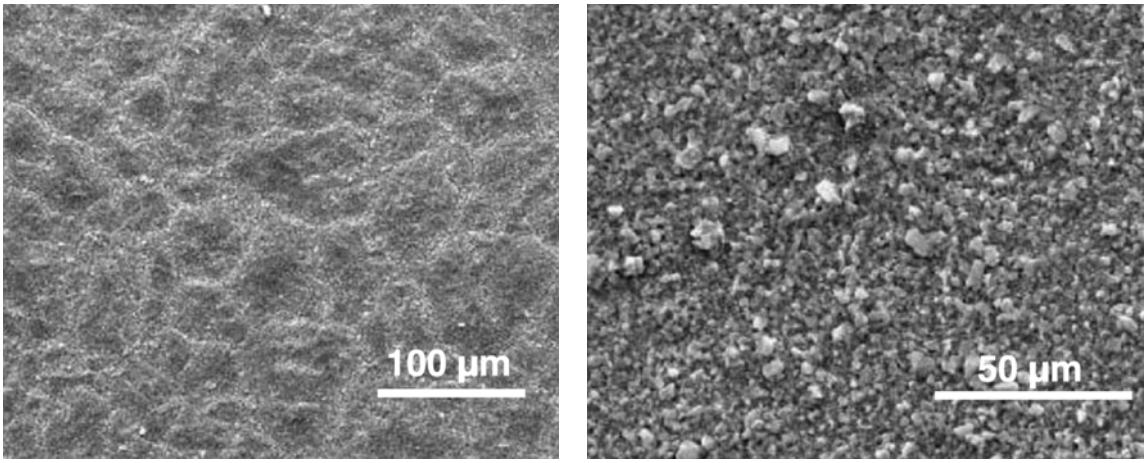

(a) (b)

Figure 2.12. Surface morphology by SEM of sintered HA coatings at 800 °C for 2 h, obtained at 800 V during: (a) 0.5 sec, (b) 3 sec [66]

In the study of Wang et al. [15], 50 V for 1 min was used to coat nanosized HA particles on a Ti substrate from acetic anhydride suspension. SEM images of the surface morphology before and after sintering are given in Figure 2.13 [15].

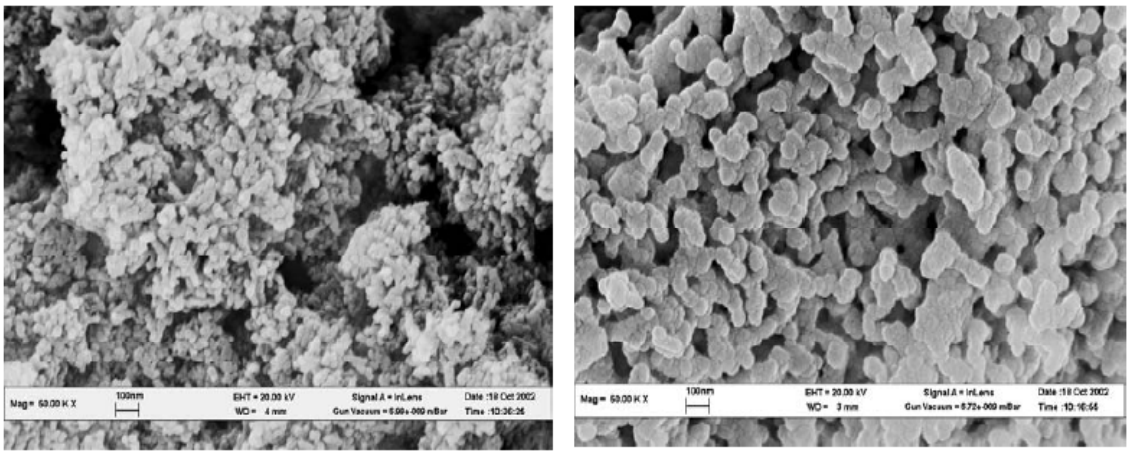

(a) (b)

Figure 2.13. SEM images of HA coating by EPD:
(a) before sintering, (b) after sintering [15]

Sintering affects the porosity of the coating layer; and porosity of HA is one of the most important factors in controlling implant performance. Higher heating temperature could be responsible for the denser microstructure (Figure 2.14), which is valid for the

enhancement of product strength [41, 51]. It has been established that an open pore structure enables penetration of bone tissue into HA ceramic and thus leads to better biointegration and mechanical stability of the implant in the bone [70]. Ma et al. [41] observed that the structure obtained from 1000 °C sintering provides the most optimum interconnected porosity (Figure 2.14). It has been reported in the literature that an open interconnected porosity structure is advantageous as it enables penetration of the tissue and hence leads to better biointegration and mechanical stability at the interface [41]. The scaffold bioactivity is not only dependent on the interconnectivity of the pores, but also the pore size [14].

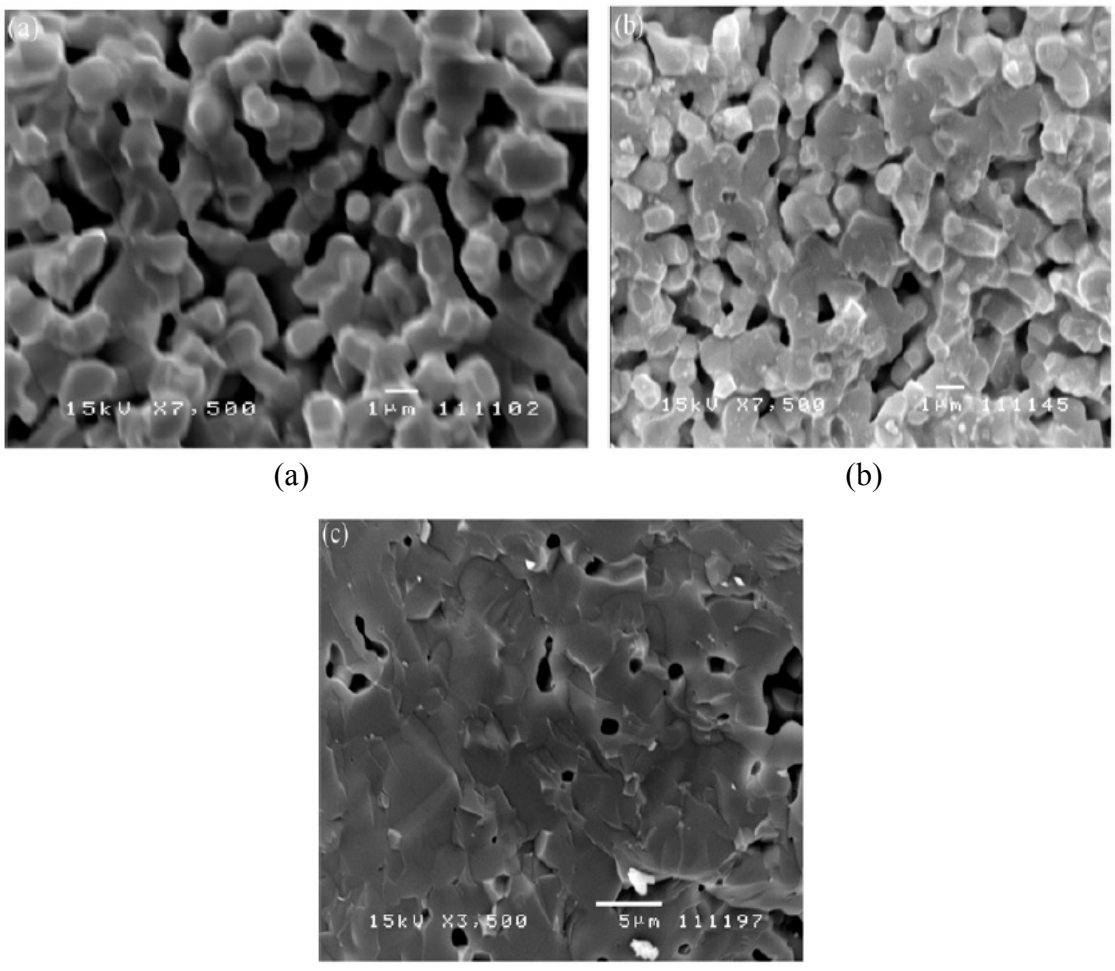

Figure 2.14. The microstructures of the HA deposits at various sintering temperatures: (a) 1000 °C, (b) 1150 °C, (c) 1300 °C [41]

Like sintering process, stable suspensions are necessary for EPD experiments. It was established that experimental conditions of powder preparation, electric field and stirring, have a marked effect on suspension stability [42]. In the study by Ma et al. [41], HA particles were deposited onto a titanium substrate via a single electrophoretic deposition process; and it is noted that the condition where the suspension is most steadily dispersed is the most optimum condition for EPD. High zeta potential and a small measured particle size desired to provide a good suspension for deposition [41].

One alternative method to obtain submicron particle suspensions is the use of dispersants. However, in the EPD of HA the dispersants are not commonly used in the conditioning of this type of suspensions because of the risk of HA contamination [42, 66]. Another option has been the selective deposition of small HA particles under the application of low voltages (< 20 V) using suspensions without dispersants [42, 66].

The other important parameter during deposition is the electric field, which is applied through either constant current density or constant voltage across the electrodes in the suspension. Particle size is an important factor for the process as the mobility of the charged particles is proportional to the size of the particles [41]. High charge/mass ratio of the colloid particles favors fast deposition of HA layer. Then the suspension can have good throwing power on to inaccessible surfaces [10]. The charges, hence the conductivity of the suspension, play an essential role and has an optimum value for the process [41].

The use of high voltages has the advantage of shorter deposition times and higher deposit thicknesses. It should be noted that in the case of relatively large particles (more than 1 μm) stirring of the suspension is usually performed in order to prevent settling. In this respect, higher voltages and smaller deposition times were found to be preferable, because shorter deposition times allow deposition without stirring. However, higher voltages usually result in significant hydrogen evolution at the cathode which, in turn, increases the porosity of the deposit. More adherent and continuous coatings with less cracking can be obtained at lower voltages [42].

The effect of the HA particle size distribution in the suspension was investigated by Zhitomirsky and Gal-Or [42]. SEM pictures of the HA deposits on TiAlV substrates at

different applied voltages are shown in Figure 2.15. As shown in this figure, by use of presedimentation and low voltages it was possible to obtain deposits which consisted only of submicron particles. Another microstructural feature was the higher coatings porosity obtained at higher voltages. Zhitomirsky and Gal-Or [42] stated that, the weight of the coating per unit surface area changed as a function of deposition time and applied voltage for experiments performed with HA suspensions.

Wang et al. [51] stated that, the quality of coatings not only depends strongly on the applied current density and the corresponding voltage but also on the conductivity and zeta potential of HA suspension as shown in Figure 2.16.

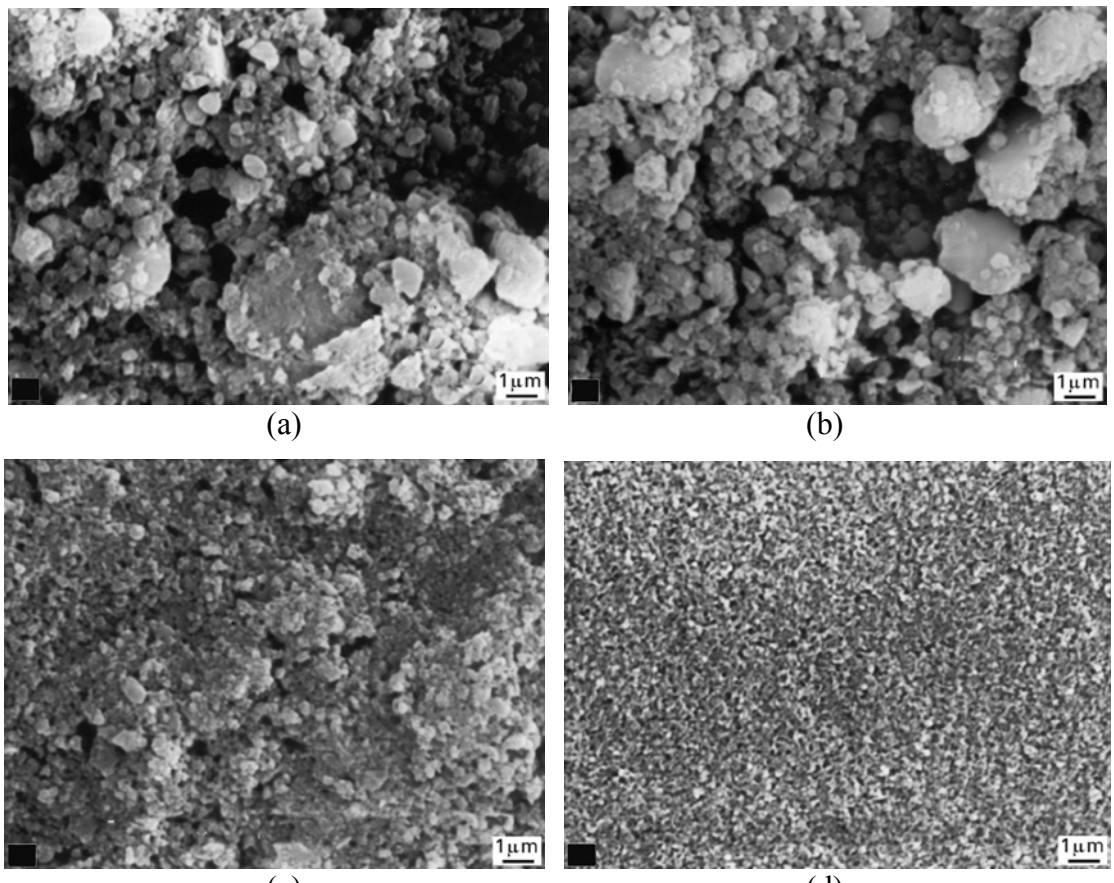

(a) (b)

(c) (d)

Figure 2.15. SEM pictures of the HA deposits on TiAlV substrates at different applied voltages: (a,b) 200 V, (c) 20 V, (d) 10 V
(a,b,c: without presedimentation, d: 1 h presedimentation) [42]

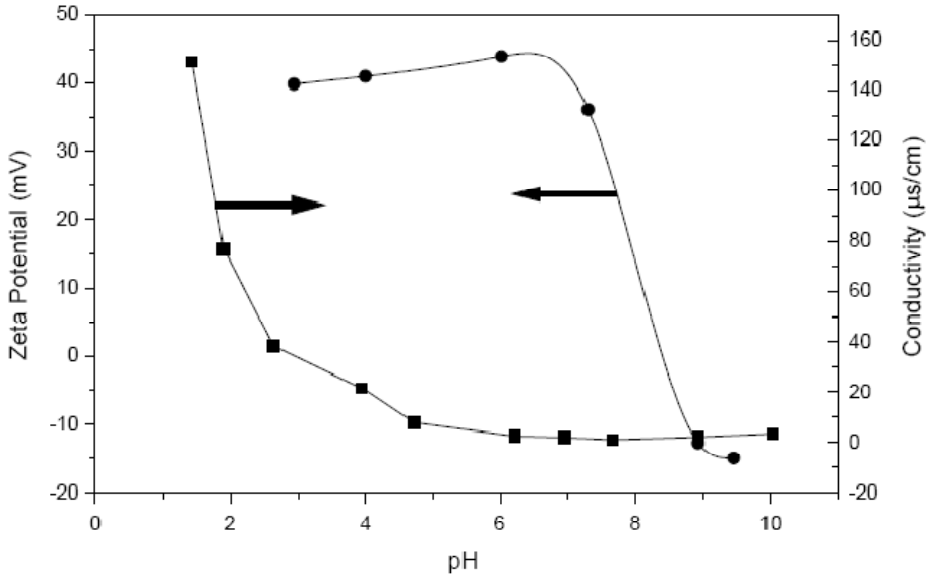

Figure 2.16. Zeta potential and conductivity of HA/ethanol suspension as a function of pH (the pH values were adjusted by using HNO_3 and NH_3) [14]

At the studies of Wei et al. [12, 75], the bonding strengths between the coating and the metal substrate, as measured by a shear strength test (Figures 2.17-2.19), were compiled in Table 2.7, which lists the adhesive strengths and their standard deviations (in MPa) of HA coatings on Ti, Ti6Al4V and 316L stainless steel sintered at various temperatures. It was found that with increasing sintering temperature, the adhesive strengths with all three metallic substrates peaked at about 900 °C, and decreased when the sintering temperature was raised further. On average, the adhesive strengths of the coatings on 316L stainless steel were much higher than those of coatings on Ti and Ti6Al4V. The highest bonding strength was obtained for the coating on 316L stainless steel sintered at 925 °C.

Table 2.7. Adhesive strengths of HA coatings on metal substrates [12]

Strength (MPa)	**875 °C**	**900 °C**	**925 °C**	**950 °C**	**975 °C**	**1000 °C**
Ti	12.4 ± 7.9	21.2 ± 10.6	14.9 ± 6.4	15.3 ± 6.3	10.9 ± 9.0	8.9 ± 4.9
Ti6Al4V	3.9 ± 3.3	17.3 ± 4.3	6.5 ± 6.2	4.1 ± 1.8	11.5 ± 3.0	11.5 ± 3.0
316L	15.4 ± 5.4	24.3 ± 9.3	25.2 ± 10.3	24.0 ± 4.7	23.0 ± 1.4	22.8 ± 1.0

Note. For comparison, the measured shear strength of cortical bone is 35 MPa

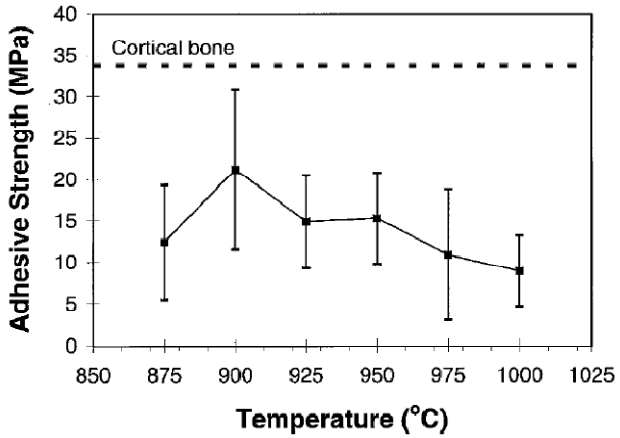

Figure 2.17. Interfacial shear strength, as a function of densification temperature for a Ti substrate [75]

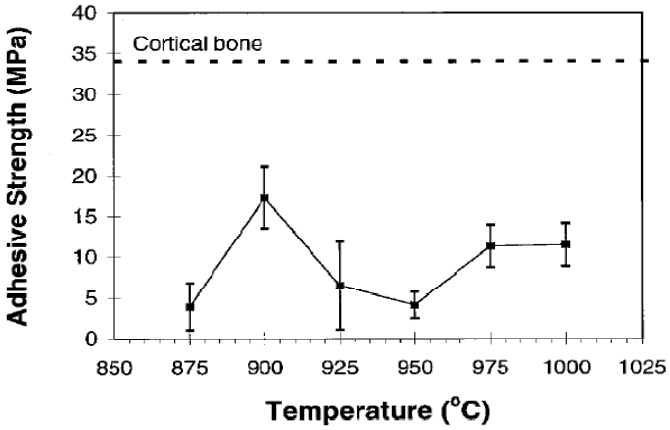

Figure 2.18. Interfacial shear strength, as a function of densification temperature for a Ti6Al4V substrate [75]

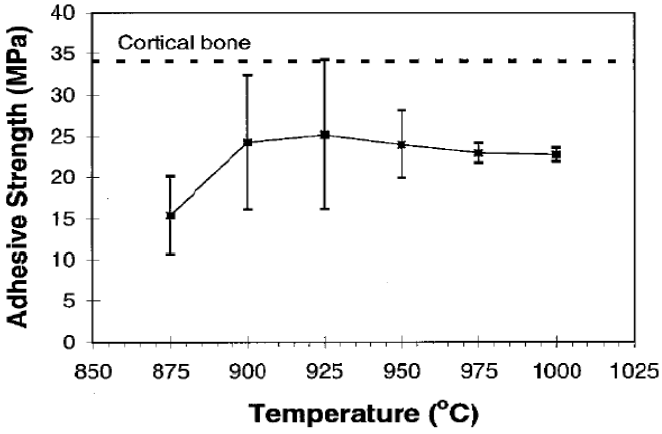

Figure 2.19. Interfacial shear strength, as a function of densification temperature for a 316L substrate [75]

3. MATERIALS AND METHODS

3.1. Production of Hydroxyapatite Powders

In this study, HA powders were produced by using two different methods, chemical synthesis or obtaining from natural resources, in order to use them as coating materials. The effects of precipitation parameters (process temperature and time) on the HA decomposition were investigated. Besides coating studies, nanosized and submicron sized HA powders, which were produced by using chemical precipitation method and by calcination of animal bone respectively, were used to prepare pellets in order to investigate their densification behavior at different sintering temperatures.

3.1.1. Chemically Synthesized Hydroxyapatite Powders

To synthesize HA powders chemically, acid-base method was performed since the reaction involves no foreign elements and the only by-product is water [74] and the procedure described by Wei [36, 74] was followed. The only difference was the aging procedure (24 h and 48 h) and temperature (30, 40 and 85 °C) applied after H_3PO_4 addition. In this procedure: 5.0 g of $Ca(OH)_2$ (~99 per cent, Merck, Germany) was dissolved in 200 ml of deionized water using a magnetic stirrer. 4.669 g of liquid H_3PO_4 (85 per cent, Merck, Germany) was added slowly (to maintain pH > 9.5-10) to the $Ca(OH)_2$ solution while the solution was continuously stirred by the magnetic stirrer. The pH value of the solution was continuously monitored using a pH meter (Orion 4 star model, Thermo, USA). Stirring was continued for 24 h (or 48 h) after H_3PO_4 addition. Then centrifugation, supernatant decantation and resuspension in deionized water were applied 5 times. After the procedure was completed, the obtained precipitates were oven-dried at 40 °C or 100 °C, and then half of them were calcined in air atmosphere at 1000 °C for 1 h or at 850 °C for 4 h (heating rate of 300 °C/h) for using in coating and densification-decomposition studies, respectively, followed by grinding by hand with an agate mortal and pestle for 20 min.

3.1.2. Naturally Derived Hydroxyapatite Powders

Naturally derived HA powders were obtained from calf femoral bones. Bones were boiled, attached to a mangle and cut with a hand saw. Both ends were cut, bone marrow was extracted and bones were cleaned from all soft tissues attached to them; middle part of the femur was taken and cut into four pieces and each of these circular pieces cut further into four [37, 81]. These pieces were heated to 850 °C for 4 h for complete removal of organic phases. The powders obtained from the pieces were used in the densification-decomposition studies. After calcination in air atmosphere at 1000 °C for 1 h (heating rate of 300 °C/h) these powders were used in coating studies.

3.2. Electrophoretic Deposition

Produced HA powders (chemically synthesized or naturally derived) and commercially obtained nanosized TiO_2 powders (Alfa Aesar, Germany) were used as coating materials. Uncalcined and calcined forms of the produced HA powders, and commercially obtained spherical-shape, anatase form of TiO_2 with the average particle size of 32 nm without any heat treatment were used in coating stage.

Schematic diagrams of the coated samples that are obtained with powders mentioned in above are illustrated in Figures 3.1-3.3. As shown in Figure 3.1, uncalcined and calcined HA powders (chemically produced and naturally derived) were used in coating studies. In these studies, the effects of calcination stage and coating parameters, such as deposition time and applied voltage, on crack occurrence were investigated. In order to increase the adhesion strength of the coating and to decrease the HA decomposition, the effects of inner TiO_2 layer between metal substrate and HA top layer were investigated. TiO_2 powders were deposited on substrates with different voltages, and then coated with HA powders as shown in Figure 3.2. And finally some preliminary studies were conducted to obtain high biocompatible and antibacterial coating. In these studies, Ca-P/TiO_2 coating surface was obtained (Figure 3.3).

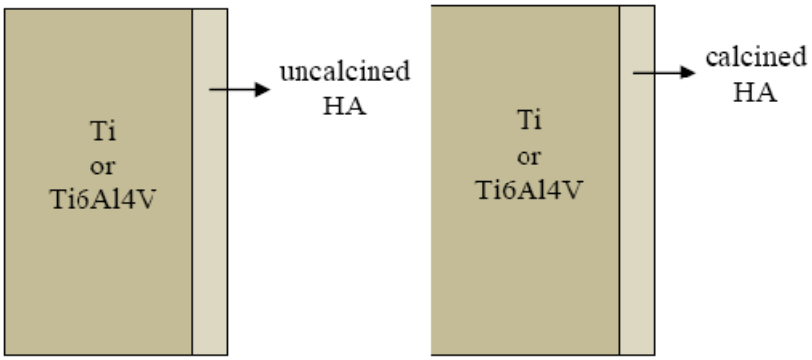

Figure 3.1. Schematic diagram of the HA coated samples

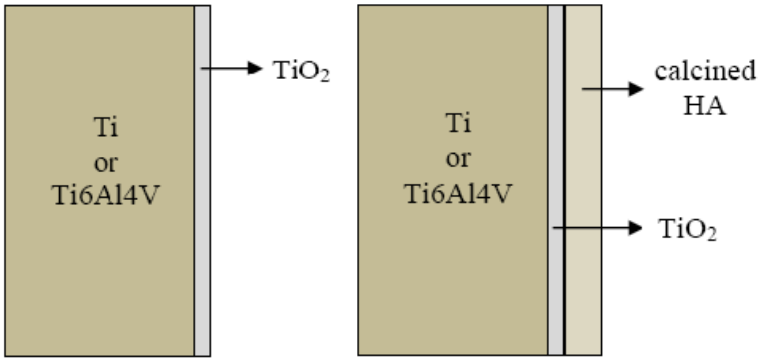

Figure 3.2. Schematic diagram of the HA coated on TiO_2 deposited samples

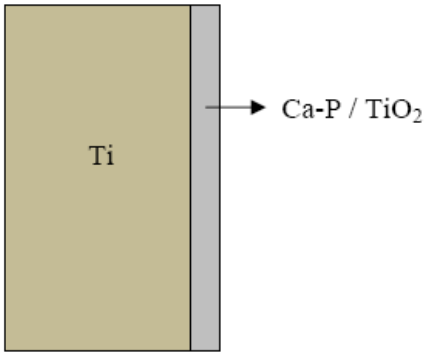

Figure 3.3. Schematic diagram of the Ca-P/TiO_2 study

1 g of HA powder was added into 100 ml ethanol (96 per cent, Merck, Germany). After magnetically stirring for 15 min, suspensions were dispersed ultrasonically for 30 min at 40 kHz in an ultrasonic bath (Everest Elektromekanik, Turkey), and then suspensions were left to rest for 30 min to eliminate the bigger or agglomerated particles

by sedimentation. Finally, the suspensions were ultrasonically dispersed again for 30 min to ensure a good dispersion of the particles [42, 66, 82]. The pH value of HA/ethanol suspension was adjusted to approximately 4, according to its zeta potential analysis results [82]. At this stage, HA particles acquired positive charge and their deposition occurred at the cathode.

The same procedure of HA coating described above was used for TiO_2 coating by EPD. The pH value of prepared TiO_2/ethanol suspension was adjusted to 3 as mentioned in the study of Lin et al. [83].

Ti and Ti6Al4V substrates were polished from 240 to 1000 grid SiC papers. Before deposition, substrates were thoroughly washed with detergent in ultrasonic bath for 30 minutes, followed by washing in acetone (extra pure, Merck, Germany) for another 20 minutes, and then passivated in 25 volumetric per cent nitric acid (65 per cent, Merck, Germany) overnight, then washed in distilled water [12, 74, 82].

The electrodes (served as anode and cathode) were placed parallel to each other in the suspension, with a separation of 10 mm approximately and connected to a DC power supply (Model AE-8150, Atto, Japan). The EPD process was performed using different voltages for different periods of time as shown at Table 3.1.

Table 3.1. Applied voltage and duration values used in the coating experiments

Coating material	**Applied voltage and duration**
HA coating	50 and 200 V for 60 sec, 50, 100 and 200 V for 30 sec.
TiO_2 coating	10, 20 and 50 V for 60sec.

After deposition, the green form coatings were dried and then sintered in a tube furnace at 1000 °C for 1 h in argon atmosphere at a heating rate of 100 °C/h and cooling rate of 50 °C/h.

3.3. Characterization

The phase purity and constitution of the produced powders and coatings were investigated to check any possible decomposition of HA by powder X-Ray Diffractometry (XRD) (Model Advance D-8, Bruker; and Model D/Max-Ultima+PC, Rigaku, Japan). The XRD data were collected at room temperature over the 2θ range of 10° - 70° at a step size of 0.02° and a count time of 0.6 sec.

The degree of HA dehydroxylation as a function of the produced parameters and calcination temperature applied was investigated by Fourier Transform Infrared Spectroscopy (FTIR) (Model 1600, Pelkin-Elmer, America) by KBr pellet method. The measurements were carried out in the transmission mode in the mid-interface range (400-4000 cm^{-1}) at the resolution of 4 cm^{-1}.

In order to determine the proper pH value used at the electrophoretic deposition, zeta potentials of the prepared coating suspensions were analyzed with respect to pH values. Zeta potential analysis (Model Nano-ZS, Malvern, England) were performed in the pH range of 3-12. NaOH and HCl were used for pH adjustment; and ethanol was used as dispersant.

The morphology and particle size of the produced uncalcined and calcined HA powders; densification behavior during sintering; and the morphology of the coating layers before and after sintering stage were observed by using SEM (Model Supra 35VP, Leo, Germany) at an accelerating voltage of 2 kV. Prior to SEM examination, all the samples were dried overnight, and sputter coated by carbon to minimize any possible surface charging effects.

Scanning electron microscopy - energy dispersive X-ray (SEM-EDX) analysis and EDX mapping were performed to visualize the occurrence of calcium, phosphor, oxygen and titanium on HA, TiO_2 and Ca-P/TiO_2 coatings.

In order to determine the effect of inner TiO_2 coating layer between Ti6Al4V substrate and HA coated layer on adhesion strength, adhesion strengths of the sintered

specimens were tested according to ASTM F1044-99 [84]. The schematic drawing of the mechanical testing apparatus and samples is given in Figure 3.4. As shown in this figure, equal sized, one coated and one uncoated Ti6Al4V plates were glued with epoxy resin (Model DP410 Scotch-weld, 3M) whose shear strength was measured as 40 MPa approximately. Testing was carried out with a universal testing machine (Model Z100, Zwick, Germany) using a 10 kN load cell and a cross-head speed of 1.0 mm/min. The adhesive strength was calculated as the peak force / fracture area. Five samples in each group were tested, and the average values were used as a final result.

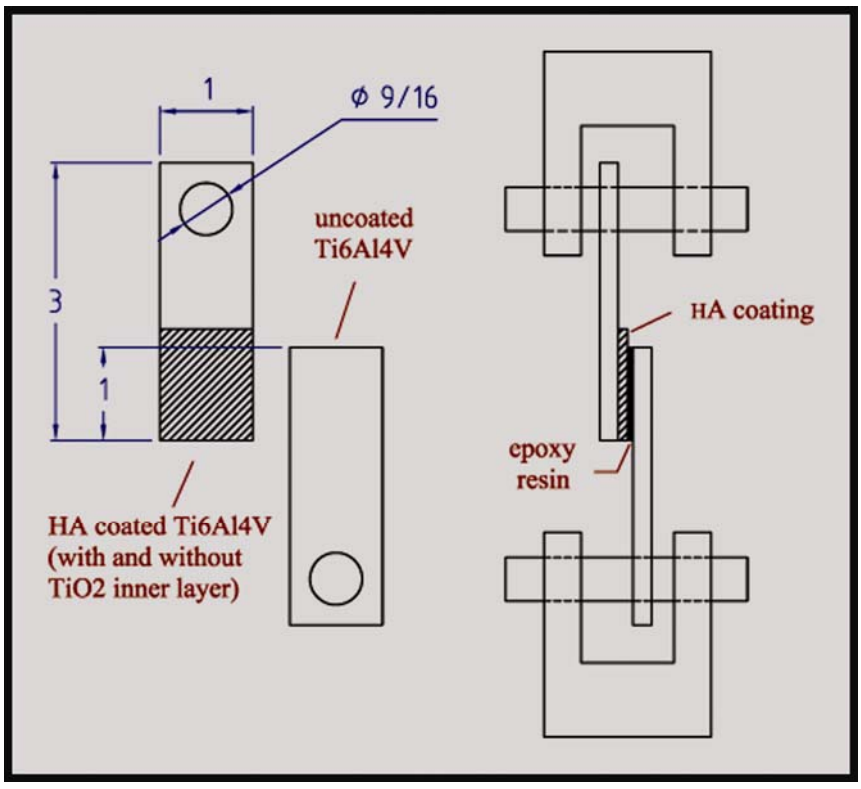

Figure 3.4. Schematic diagram of the mechanical testing apparatus and samles
(1 unit = 1 in.= 25.40 mm)

Compression and Vickers microhardness tests were conducted on the sintered HA pellets obtained from chemically synthesized nanosized, naturally derived sub-micron sized HA, and mixture of both powders in equal proportions. The samples obtained from the three different batches were compared.

4. RESULTS AND DISCUSSION

The first part of the experimental studies deals with the production of HA powders. The second part mainly focuses on the coating of the produced HA powders on Ti and Ti6Al4V substrates.

4.1. Production of Hydroxyapatite Powders

Studies were conducted to produce HA powders to use in obtaining HA coatings. For this purpose, the best suitable parameters for this process have been investigated in the current study, since processing time and precipitation kinetics are critical for the purity of the HA product and its crystallographic characteristics [7, 85, 86].

4.1.1. Effects of Precipitation Temperature and Time on the Hydroxyapatite Decomposition

In the current study, HA powders that were synthesized from phosphoric acid and calcium hydroxide using different process temperature and time (at 85 °C for 10 min and 24 h, at 30 °C for 24 h, and at 40 °C for 24 h and 48 h) were characterized with respect to their decomposition behavior.

The powders synthesized by setting the temperature of the reactant solutions at 85 °C were oven-dried at 100 °C for 24 h. Half of obtained powders were calcined in air atmosphere at 1000 °C for 1 h (heating rate of 300 °C/h).

XRD spectrum and results of phase identification for these dried and calcined powders (synthesized at 85 °C for 10 min and 24 h) are presented in Figures 4.1 and 4.2, respectively. As shown in Figures 4.1 and 4.2, heating of the dried powders in air atmosphere at 1000 °C for 1 h caused them to crystallize. The observed phases in the chemically synthesized dried powders were determined by powder XRD to be completely HA (International Centre of Diffraction Data (ICDD), Powder Diffraction File (PDF) No:

84-1998). For the calcined powders, besides primarily HA peaks, there were only a few peaks of calcium oxide (CaO) [87].

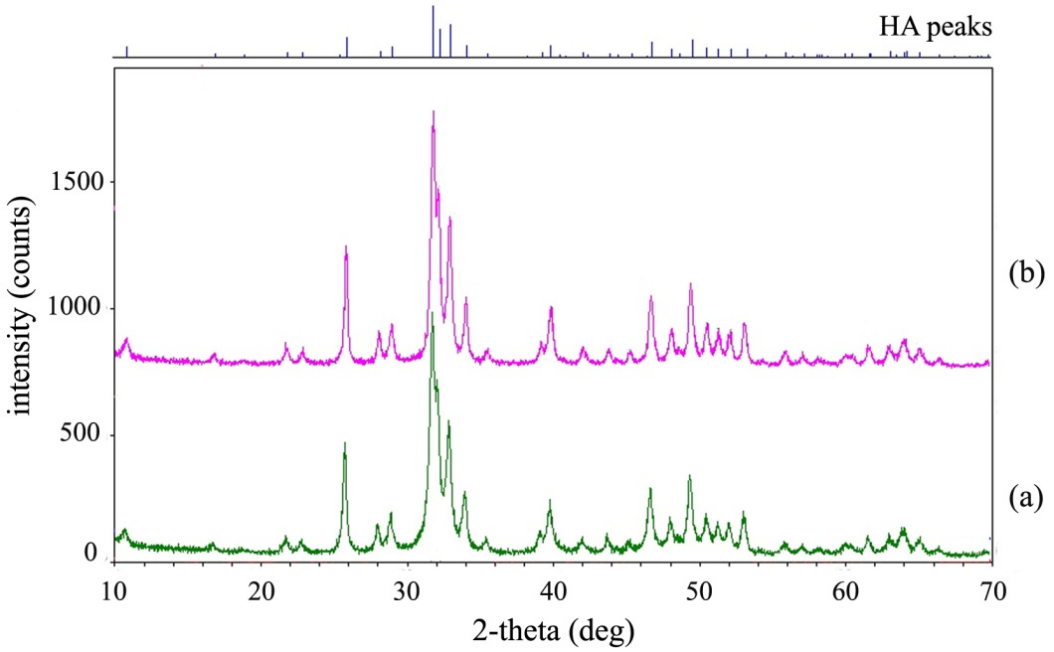

Figure 4.1. XRD spectra of produced powders (dried) at 85 °C for: (a) 10 min, (b) 24 h

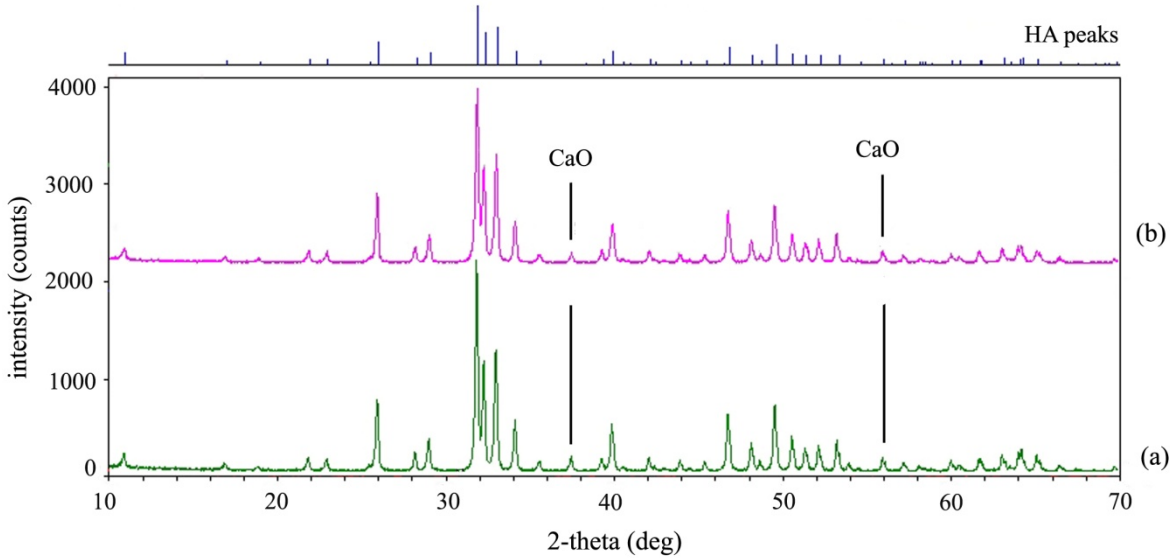

Figure 4.2. XRD spectra of produced powders (calcined at 1000 °C for 1 h) at 85 °C for: (a) 10 min, (b) 24 h

The FTIR spectra of synthesized HA samples are shown in Figure 4.3. The IR spectra of the biomaterial show the absorption bands at 3572 cm^{-1} and 3433 cm^{-1} which correspond to stretching mode of hydroxyl group. The hydroxyl vibration mode is found to be present near 632 cm^{-1}. The band due to ν_3 vibrations of hydroxyl group is present at 1625 cm^{-1}, whereas the bands at 1636 cm^{-1} are due to NO_3 group, and the bands around 2320 and 2360 cm^{-1} are due to CO_2 group. The absorption bands appearing at 418, 575 and 601 cm^{-1} can be attributed to the ν_4 fundamental bending mode of PO_4^{3-} functional group and the peaks in the range 1089-1039 cm^{-1} are due to ν_3 vibrations of PO_4^{3-}. The bands at 974 and 963 cm^{-1} are due to ν_1 fundamental mode of PO_4^{3-}. The IR spectrum of the biomaterial synthesized shows additional absorption band at 3644 cm^{-1} which corresponds to hydroxyl stretching mode associated with surface P-OH groups and presence of small amount of CO_3 can be evidenced by the bands appearing at 1459 cm^{-1} showing the formation of carbonate apatite [88, 89]. This is attributed to the trace impurities present in the starting material. The symmetric and anti-symmetric stretching of the PO_4 group (at 1096, 1046, 963, 604 and 576 cm^{-1}) and the stretching and vibrational modes of the O-H group at 3571 and 639 cm^{-1} showed the presence of HA phase in support of the XRD data.

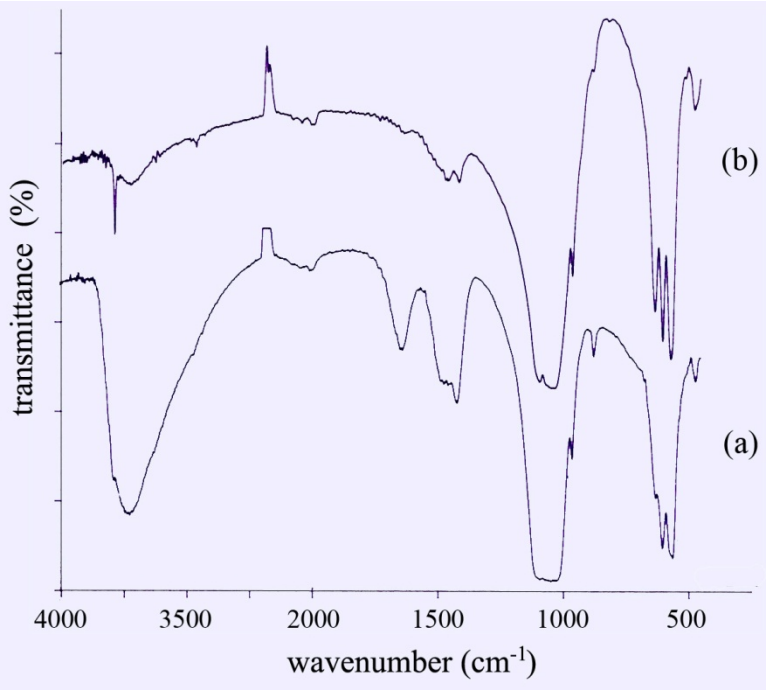

Figure 4.3. FTIR spectra of produced powders at 85 °C for 10 min:
(a) dried, (b) calcined at 1000 °C for 1 h

In the next study, the powders synthesized at 30 °C for 24 h were examined. The produced powders were oven-dried at 80 °C for 24 h, and calcined in air atmosphere at 1000 °C for 1 h (heating rate of 300 °C/h); and then examined to determine the phase purity and constitution (by XRD), and morphology and particle size (by SEM) of the synthesized powders.

XRD spectra and results of phase identification for dried and calcined powders are presented in Figure 4.4. The observed phases in the dried powders were determined by powder XRD to be completely HA (ICDD PDF No: 84-1998). For the calcined powders, besides primarily HA peaks, there were only a few peaks of TCP.

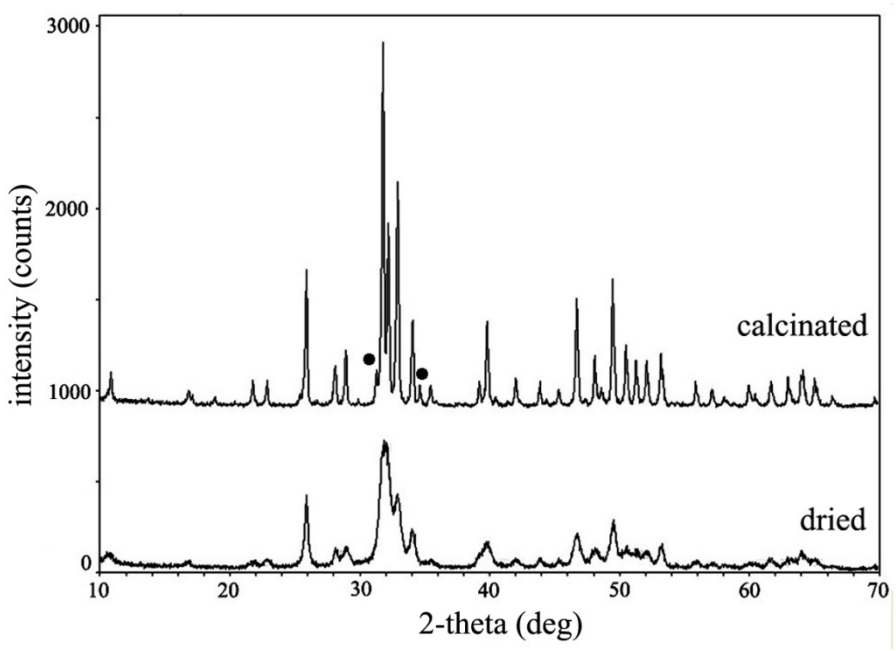

Figure 4.4. XRD spectra of synthesized powders at 30 °C for 24 h by acid base method (● is used for TCP, all unsigned peaks are HA)

SEM micrograph of dried powders that were synthesized at 30 °C for 24 h by acid-base method shown in Figure 4.5a reveals that the acid-base method produced needle-like nano-particles (about 120 nm × 40 nm, aspect ratio ~ 3:1). Further calcination of these particles at 1000 °C for 1 h, coarsened them into nodular-like particles (about 180 nm × 150 nm, aspect ratio ~ 1.2:1) (Figure 4.5b) [82].

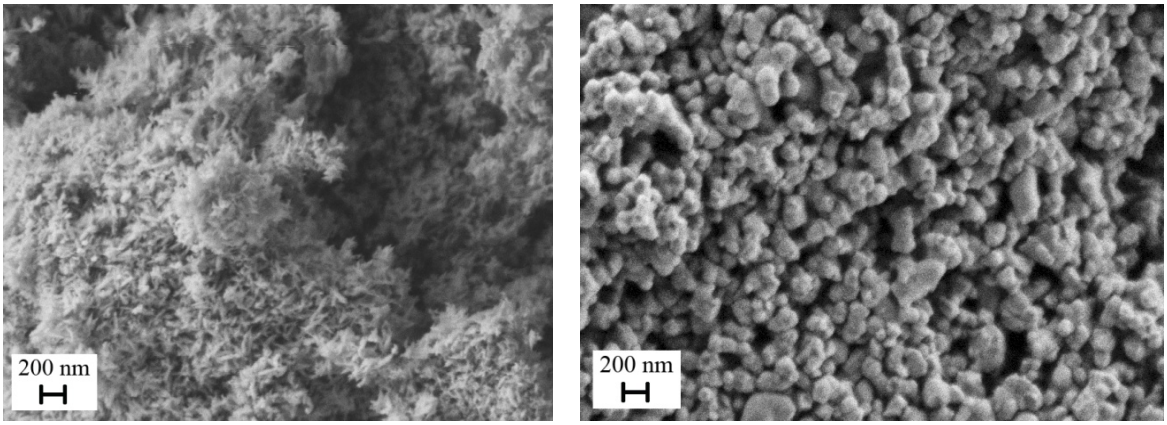

(a) (b)

Figure 4.5. SEM micrograph (equal magnification; scale bar=200 nm) of synthesized HA powders at 30 °C for 24 h: (a) dried powders, (b) calcined powders

In the final part of this study, both chemically synthesized and naturally derived powders were examined to determine the phase purity and constitution, and morphology and particle size of the produced powders. Chemically synthesized (produced at 40 °C for 24 h), and naturally derived (from calf bone) powders were calcined at 850 °C for 4 h. Three batches of powders have been prepared. The first containing only synthetically produced HA and the second one containing only HA naturally obtained from calf femoral bone. The third batch is a mixture of both powders in equal proportions. Powders from the three different batches have first been compacted using a uniaxial press into cylindrical specimen in a steel die with a pressure of 80 MPa. The pressed cylindrical specimens have further been compacted in a cold isostatic press at 400 MPa. The prepared specimens were sintered at 900 °C and 1200 °C for 2 h with a heating and cooling rate of 100 °C/h in air atmosphere. The phase purity and constitution of the powders and sintered batches were investigated to check any possible decomposition of HA by XRD, and the morphology and particle size of the produced HA powders were observed by using SEM.

XRD spectra of both powders produced naturally and synthetically clearly show that the only existing phase is HA in both calcined powders, as shown in Figure 4.6. Codes “N” and “S” are used for naturally produced and chemically synthesized powders, respectively.

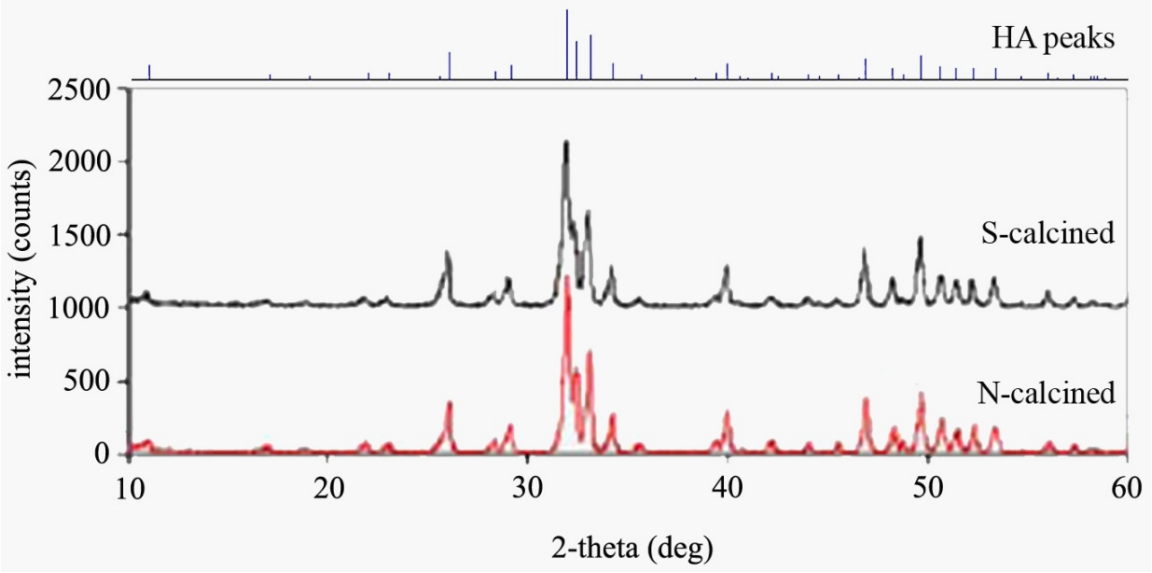

Figure 4.6. XRD spectra of naturally and synthetically produced powders after calcination

Regarding the morphology of the powders it can be stated that both kind of powders have nearly nodular shapes and an even particle size distribution within themselves (Figure 4.7). The particle size of the synthetic powder is in the range of 50 to 100 nm whereas the particle size of the natural HA is of the order of 1 μm.

To determine the phase purity of HA at the selected sintering temperatures (900 °C and 1200 °C) XRD data were taken for all the three batches at both of the temperatures after sintering. XRD spectra and results of phase identification for sintered batches are presented in Figure 4.8. The code “NS” refers to the mixture of naturally produced and chemically synthesized HA in equal proportions. The observed phases in all the samples were determined by powder XRD to be completely HA (ICDD PDF No: 00-009-0432).

The spectra obviously show that both kinds of powders are pure HA both at 900 and 1200 °C as shown in Figure 4.8. There is no decomposition of HA into TCP even at 1200 °C for none of the samples. Therefore, it can be stated that a sintering temperature as high as 1200 °C can safely be chosen for HA without any risk of decomposition. This result is consistent with the data found in literature [90].

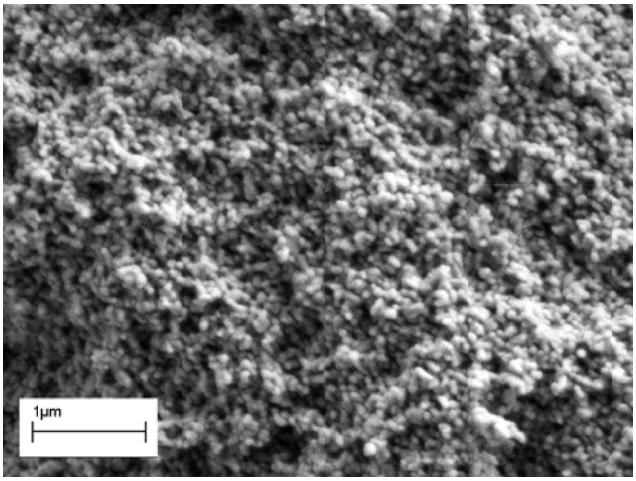

(a)

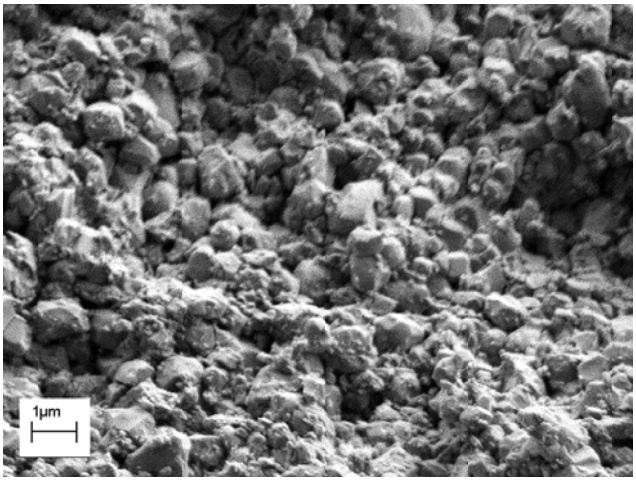

(b)

(c)

Figure 4.7. SEM images of the HA samples after cold isostatic pressing (calcined powders at 850 °C for 4 h): (a) synthetically produced, (b) naturally produced, (c) mixture of the naturally and synthetically produced [91]

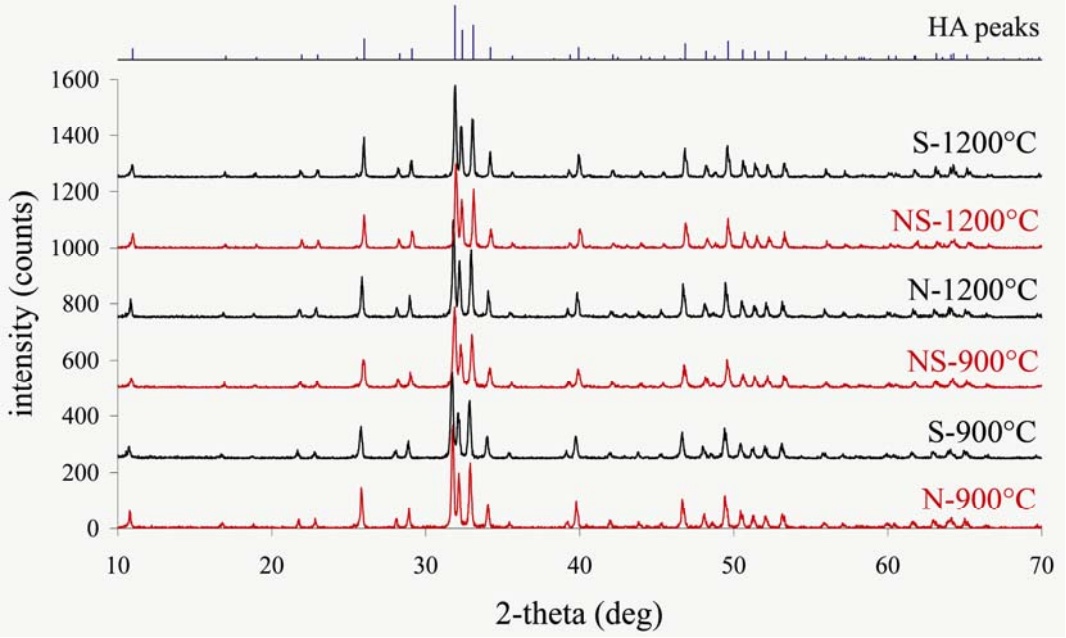

Figure 4.8. XRD spectra of the three different samples sintered at two different temperatures

4.1.2. Densification Behavior of Produced Hydroxyapatite Powders

The aim of this study is to investigate the densification, sintering behavior and mechanical properties of chemically synthesized and naturally derived powders, and their mixture in equal proportions. Prepared HA powders mentioned above (calcined at 850 °C for 4 h, uniaxially pressed at 80 MPa, cold isostatically pressed at 400 MPa, sintered at 900 °C and 1200 °C for 2 h) were used in this study. The densification behavior of the specimens (chemically synthesized, naturally derived, and their mixture in equal proportions) during sintering were observed by using SEM. Compression and Vickers microhardness tests were conducted on the sintered samples. The samples from the three different batches were compared based on their SEM pictures.

The specimen prepared from both of the powders and their mixture were isostatically pressed. In order to gain deeper insight into the compaction behavior of the powders the SEM images were taken (Figure 4.7). As seen in Figure 4.7, all of the three different batches of powders are compacted. However, the mixed batch, as shown in Figure 4.7c, showed an inhomogeneous distribution of the relatively bigger particles of natural HA in

the smaller particles of synthetic HA. This can be a result of improper mixing prior to compaction as well as a result of agglomeration of particles of similar sizes.

Effects of the different sintering temperatures on densification were determined by the observation of the SEM images of the samples sintered at 900 °C and 1200 °C. The SEM images of the sintered samples indicated that sintering is not fully achieved at 900 °C, as seen in Figure 4.9. However, at 1200 °C both the pure samples as well as the mixture are completely sintered (Figure 4.10).

There is a significant difference in the SEM images of the natural and synthetic powders. The synthetic powders produce a smooth fracture surface without obvious grain boundaries as opposed to the natural powders. This is due to the fact that the densification level depends predominantly on the surface area of the HA powder. Since smaller sized powders have greater surface area the synthetically produced HA powders exhibit better sintering characteristics. This is based on the assumption that the surface roughness is similar for both powders which can be justified by the observation of the SEM images.

The compaction behavior of the sintered bodies as observed on the SEM images mainly depends on the homogeneity and the particle size distribution of the precursor powders, which is clear on Figures 4.10a and 4.10b. Since the samples on Figures 4.10a and 4.10b are produced of pure powders they show a good densification behavior. However, there is an obvious porosity in Figure 4.10c which shows the sintered body produced from two different powders of significantly different particle sizes. Therefore, it can be stated that an improved packing homogeneity leads to an improved sinterability in the form of a higher densification after sintering at a given sintering temperature.

The results of the compression measurements to obtain the mechanical properties of the batches prepared from different powders seem to be consistent with the above observation based on the SEM images in Figure 4.10. Table 4.1 shows the compressive strengths of the samples of different compositions after sintering at different temperatures. An increase in the sintering temperature clearly enhances the compressive strength for both batches prepared using pure powders. However, the mixed batches have a very low compressive strength as compared to the other two samples.

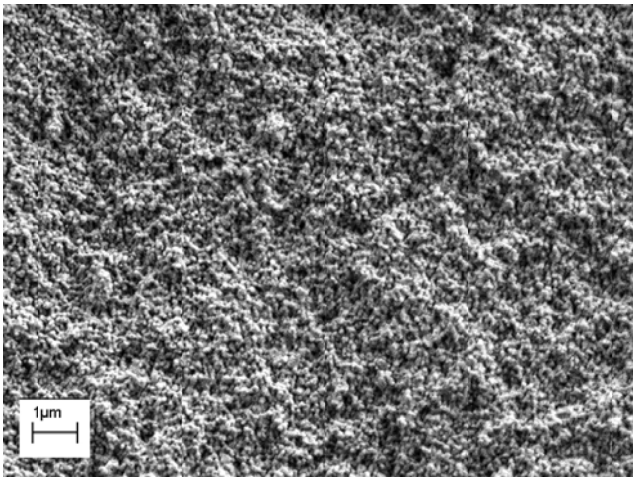

(a)

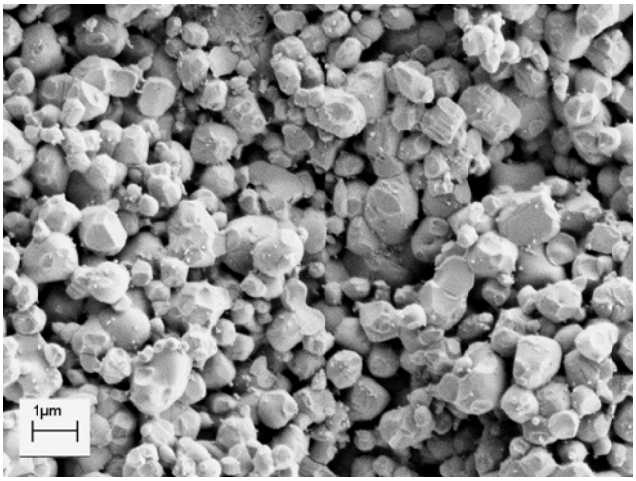

(b)

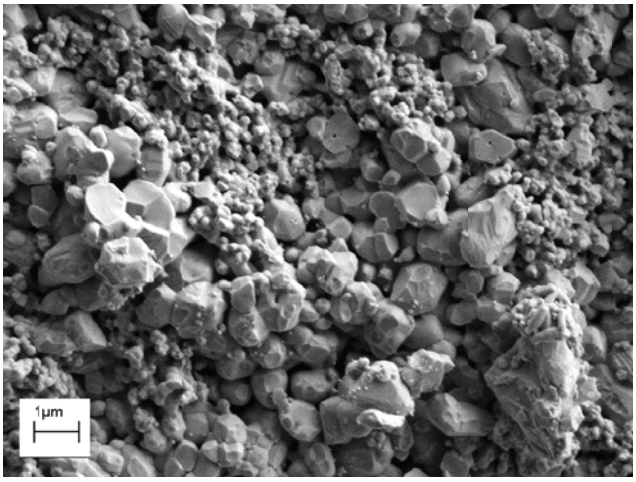

(c)

Figure 4.9. SEM images of the HA samples sintered at 900 °C: (a) synthetically produced, (b) naturally produced, (c) mixture of the synthetically and naturally produced [91]

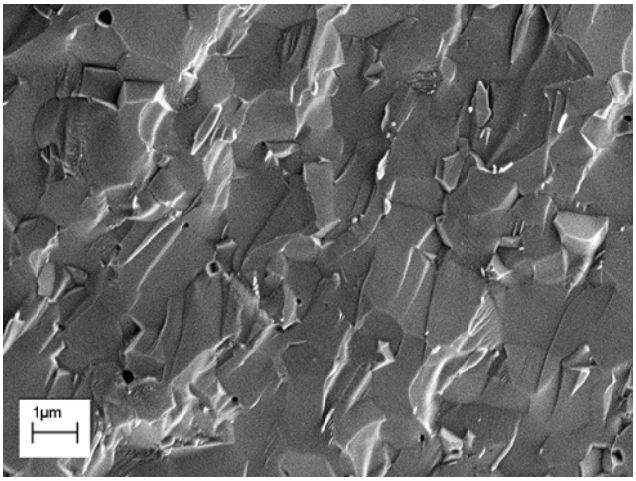

(a)

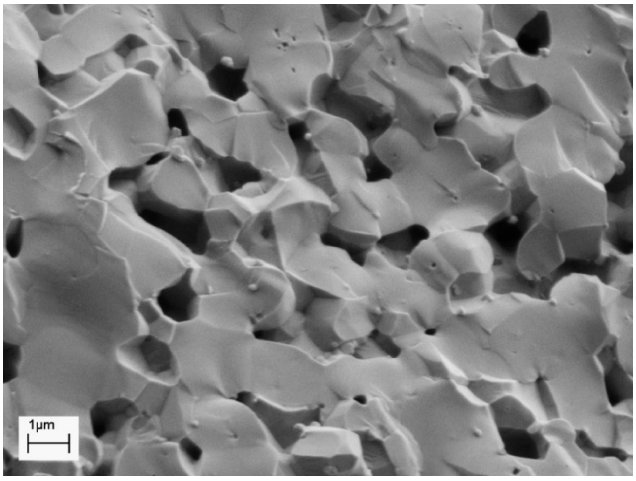

(b)

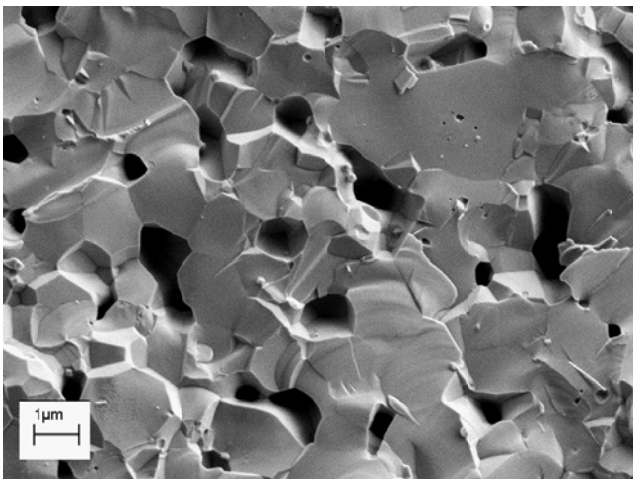

(c)

Figure 4.10. SEM images of the HA samples sintered at 1200 °C: (a) synthetically produced, (b) naturally produced, (c) mixture of the synthetically and naturally produced

Table 4.1. Compression strengths of the samples [91]

Specimen	Compression strength (MPa)
S-900	119
N-900	117
NS-900	54
S-1200	297
N-1200	268
NS-1200	112

The microhardness measurements are summarized in Figure 4.11. Increasing the sintering temperature increases the hardness for all set of powder compact samples. However, increase in the hardness of the synthetically produced HA is more pronounced than the others.

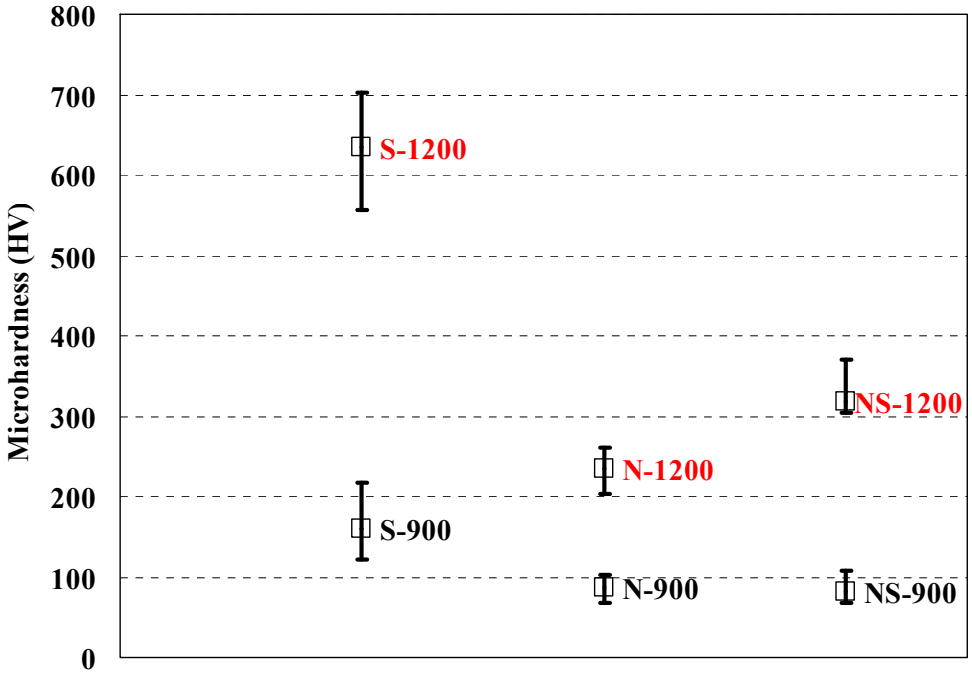

Figure 4.11. Microhardness measurements of the samples [91]

4.2. Electrophoretic Deposition of Hydroxyapatite Powders on Metallic Substrates

Although the EPD exhibits some advantages over other alternative processes (as mentioned in Section 2), cracks on coating surfaces may occur after the process of deposition, drying and sintering [12, 74]. To prevent crack occurrence on coating surfaces, the effects of HA powders produced by a variety of methods [74] and effects of dual HA coating [12] were investigated by Wei et al. In [74], acid-base, calcium acetate and metathesis methods were applied to produce HA powders in order to be used in the coating stage, and crack occurrence on coating surfaces were investigated. It was revealed that the acid-base method produced severely cracked coatings, the calcium acetate powder produced slightly cracked coatings, and the metathesis powder produced crack-free coatings [74]. Although crack occurrence was not observed on coating surface when the metathesis method was used for the production of HA powders, this method requires a long aging process (20-100 days) which is necessary for the production of powder. In addition to that, impurities, which occur along with HA, must be removed.

The coating surfaces obtained by the methods mentioned above were investigated before sintering process [12, 74]. The metathesis method produces crack-free coating surface in this stage, however cracks were observed on the coating surface after sintering [12, 74]. To prevent crack occurrence after sintering, the application of dual coating was studied [12]. For this purpose, a cycle consisting of consecutive coating and sintering steps were applied twice, and it was observed that surface cracks, occurring after the first coating layer were covered by the second coating layer [12]. Although obtaining a crack-free coating surface using dual coating is possible, another sintering stage must follow the second coating step which doubles the processing time.

In the scope of this thesis, coating parameters, such as deposition time and applied voltage, as well as the effect of calcination on crack occurrence were investigated The produced HA powders were further used in the studies regarding the coating of metallic substrates. In order to increase the adhesion strength of the whole coating and to decrease the HA decomposition, the inner layer between HA coating layer and substrate was investigated. TiO_2 was used as the inner coating layer. Preliminary studies were conducted

to obtain Ca-P/TiO_2 coating surface expecting to produce a biocompatible and antibacterial coating

4.2.1. Crack Occurrence on Coating Surface

In the current study which is related to decreasing or eliminating the crack occurrence in coating surfaces, effects of voltage (applied at deposition stage), and calcination (applied at HA powder preparation stage) on crack occurrence were investigated. In the former study, different voltages as 25, 50, 100 V were applied at deposition stage. And in the latter one, uncalcined (chemically synthesized) and calcined (chemically synthesized and naturally derived) HA powders were used as coating material.

Before starting the deposition process, zeta potential analysis was performed, and zeta potential analysis with respect to pH values for HA/ethanol suspensions were obtained (Figure 4.12) to determine the proper pH value for EPD. Zeta potential values of all samples were over 30 mV for the pH range of 3-5 (similar to Figure 4.12). Since high absolute zeta potential value indicates the presence of a well-dispersed suspension [51], pH values of all suspensions were adjusted to approximately 4 to investigate the calcination effects on EPD. At this stage, HA particles acquired positive charge and their deposition occurred at the cathode.

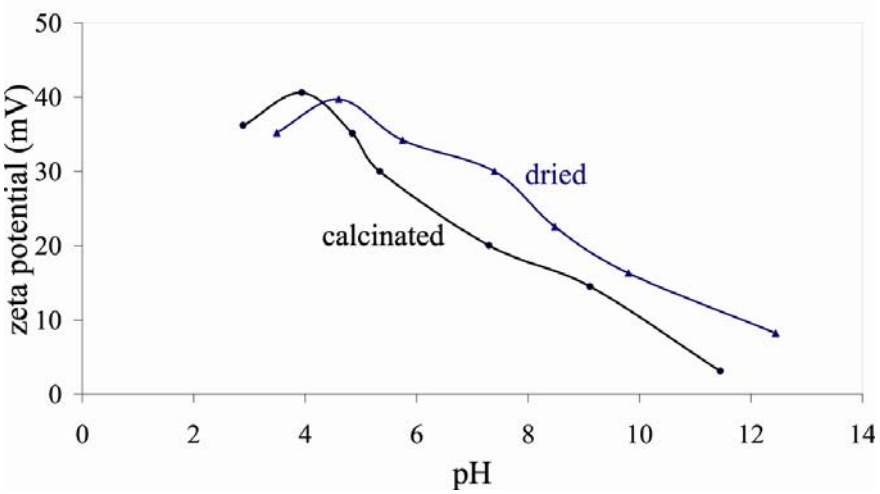

Figure 4.12. Zeta potential analysis as a function of pH for HA/ethanol suspension (chemically synthesized HA powders - dried and calcined at 1000 °C for 1 h)

To investigate the effect of voltage on crack occurrence, HA powders synthesized using different parameters were coated under application of various voltages. First, uncalcined HA nanopowders that were synthesized at 85 °C for 24 h were deposited by applying 50 and 100 V for 30 sec. After drying, the deposited specimens were examined by SEM; and as shown in Figure 4.13, surface cracks were seen on all the specimens obtained by both parameters. Moreover, the results of the experiments state that the tendency of crack occurrence increases with the applied voltage. Next, uncalcined HA nanopowders (synthesized at 40 °C for 24 h) were deposited by applying 25 and 50 V for 60 sec. After sintering at 1000 °C for 2 h, the coated specimens were examined by SEM; and as shown in Figure 4.14, similar results to the previous one were obtained.

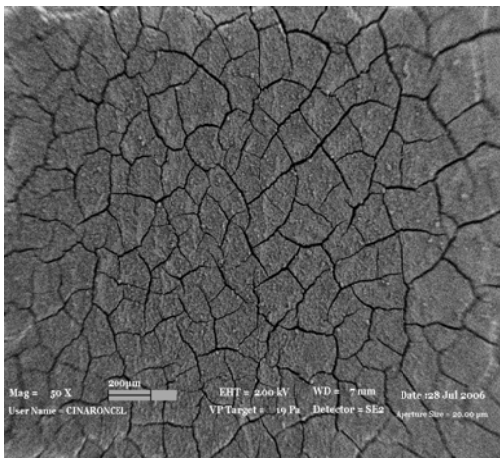

(a)

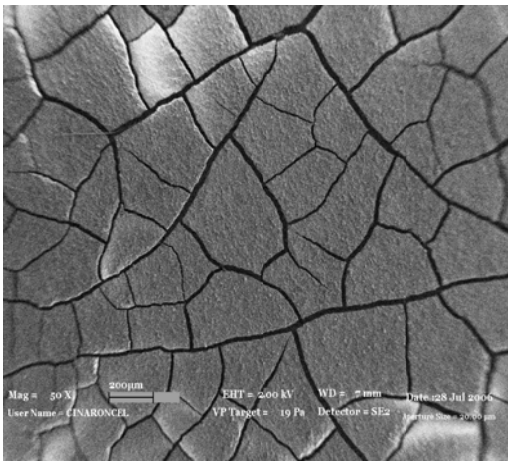

(b)

Figure 4.13. SEM images (in equal magnification) of the HA deposits (before sintering stage) using dried nanopowders synthesized at 85 °C for 24 h:
(a) 50 V for 30 sec, (b) 100 V for 30 sec [92]

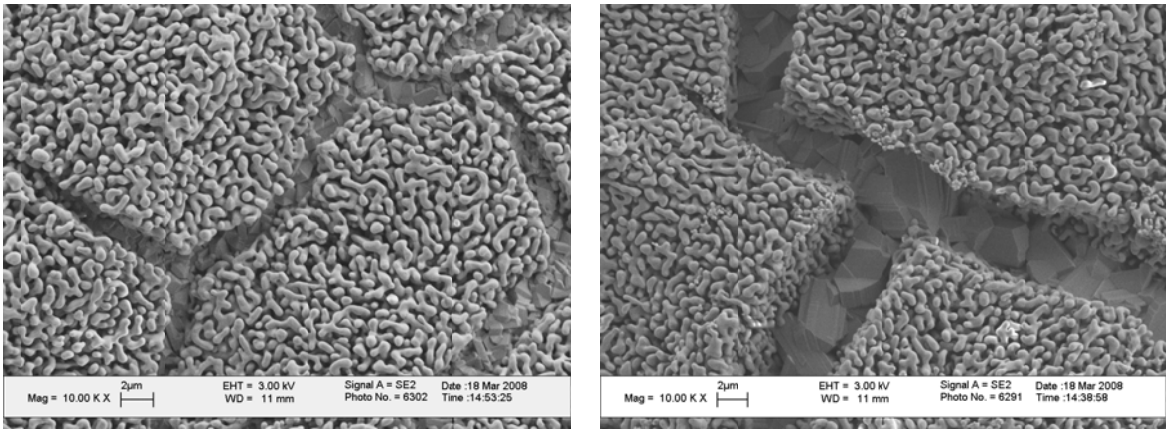

(a) (b)

Figure 4.14. SEM images (in equal magnification) of the HA deposits (after sintering stage) using dried nanopowders synthesized at 40 °C for 24 h:
(a) 25 V for 60 sec, (b) 50 V for 60 sec

In the investigation of effect of calcination (applied in preparing HA powder preparation stage) on crack occurrence, uncalcined (chemically synthesized) and calcined (chemically synthesized and naturally derived) HA powders were used in the EPD as coating material. Schematic diagram of this study is presented in Figure 3.1.

Chemically synthesized HA powders were produced at 30 °C for 24 h; and half of them were calcined at 1000 °C for 1 h. Naturally derived HA from calf bone were heated to 850 °C for 4 h for complete removal of organic phases, and then calcined at 1000 °C for 1 h. Obtained powders were deposited under a constant voltage of 50 V for 60 sec. After deposition, the green form coatings were dried at room temperature in air, and then sintered in a tube furnace at 1000 °C for 1 h in argon atmosphere. The specimens obtained before and after sintering stage were investigated to crack occurrence by SEM.

The effects of calcination on crack occurrence (before sintering stage) are shown in the SEM micrographs of Figures 4.15 and 4.16 reveal that the use of uncalcined powders at EPD caused cracks on coating surface (Figure 4.15a) whereas, calcined powders exhibits crack-free surfaces (Figures 4.15b and 4.16) even after sintering stage (Figure 4.17a). SEM micrograph of the sintered coating surface at 1000 °C for 1 h (Figure 4.17b) presented bonding between particles [82].

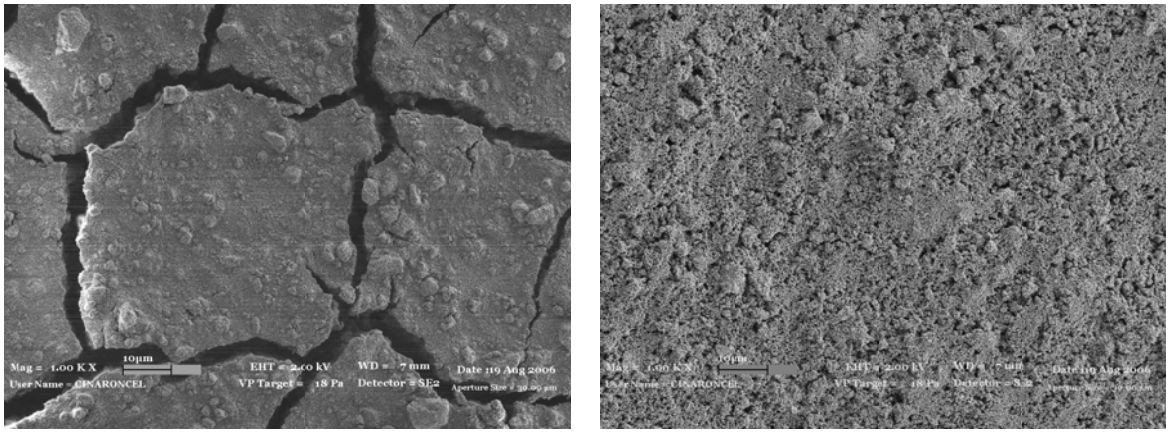

(a) (b)

Figure 4.15. SEM micrograph (equal magnification; scale bar=10 μm) of the HA deposits (before sintering stage) using synthesized HA powders at 30 °C for 24 h:
(a) dried powders, (b) calcined powders

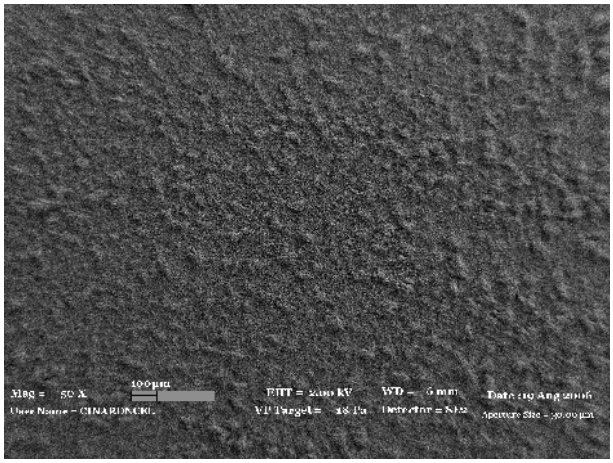

Figure 4.16. SEM pictures of the HA deposits (before sintering stage) using naturally derived calcined powders

Cracks, seen in Figures 4.13 and 4.15a, arise as a result of shrinkage during drying. Drying shrinkage is minimized by the use of regularly shaped particles that can pack efficiently, and large particle size distributions for gap-graded efficient packing [74]. Cracking susceptibility can be dependent on the shape and size of the HA particles, and dehydration of powders in calcination stage.

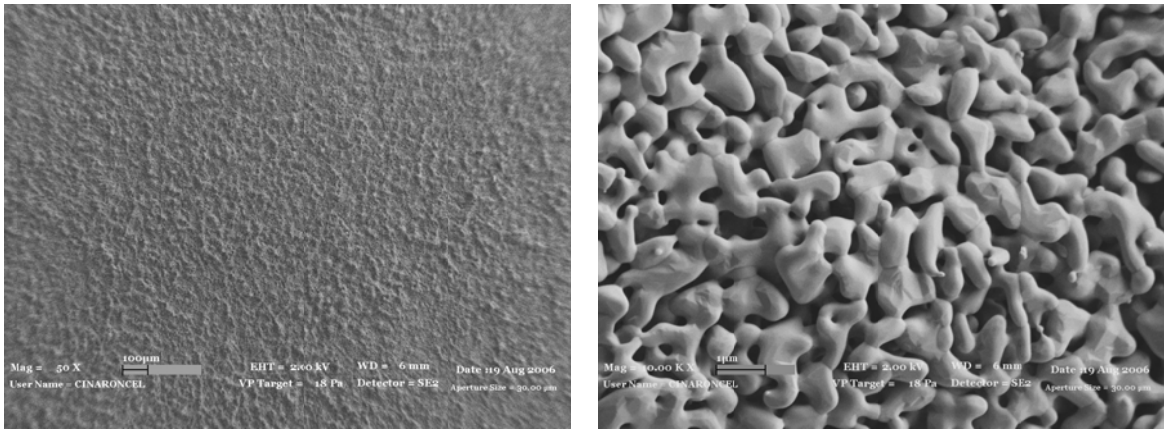

(a) (b)

Figure 4.17. SEM micrograph (in different magnification) of the HA deposits (after sintering stage) using synthesized HA powders at 30 °C for 24 h: (a) calcined powders, crack-free coating surface, (b) calcined powders, bonding between the particles

4.2.2. Effects of Titanium Dioxide Inner Layer on Adhesion Strength and Hydroxyapatite Decomposition

The aim of this study was to produce HA coating on Ti6Al4V substrate by EPD method with improved coating adhesion and decreased HA decomposition, and to investigate the effects of the inner TiO_2 layer on them. (Schematic diagram of the HA coated on TiO_2 deposited samples are given in Figure 3.2.)

HA powders were synthesized at 40 °C for 48 h using acid-base method, and calcined in air atmosphere at 1000 °C for 1 h to be use in EPD process in order to obtain crack-free coating surface as stated in the previous study (Section 4.2.1). Before the deposition process, calcined powders were analyzed by XRD to check phase purity and constitution; it was determined that XRD peaks of calcined powders were completely matched with the HA peaks (ICDD PDF No: 09-0432), and no other phases were observed. The pH value of HA/ethanol suspension was adjusted to approximately 4, according to its zeta potential analysis which was obtained in the previous study (Section 4.2.1, Figure 4.12). The EPD process was performed under a constant voltage of 200 V for 60 sec for HA coating. After sintering in a tube furnace at 1000 °C for 1 h in argon atmosphere, surface morphology of HA coating was investigated and SEM micrographs of the coating

surface and section are presented in Figure 4.18 to illustrate bonding between the particles, crack-free surface and coating thickness. As shown in Figure 4.18, crack-free HA coating (top-right corner) with thickness of about 30 µm (bottom-right corner) was obtained.

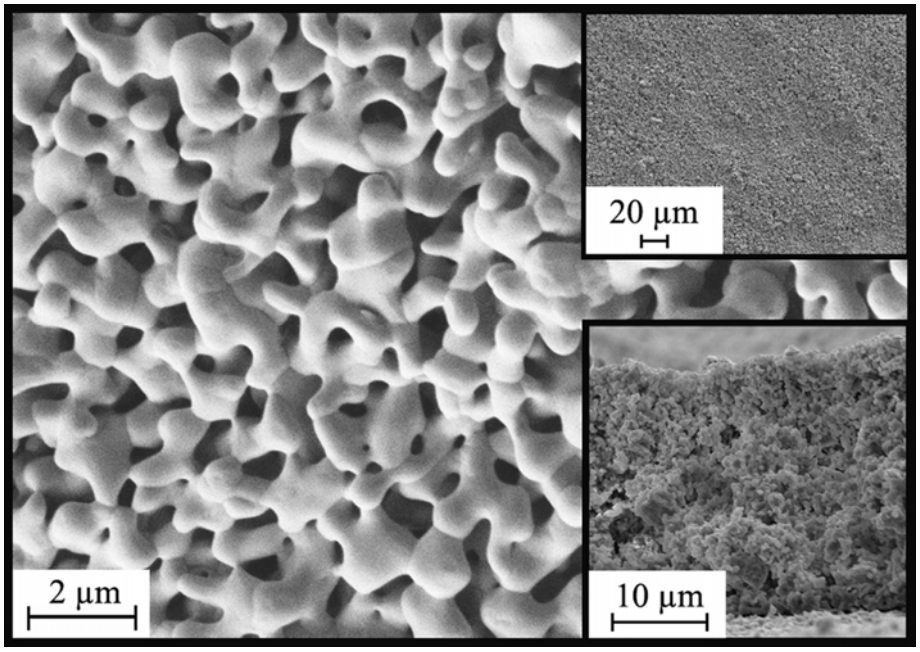

Figure 4.18. SEM micrograph of HA coating without TiO_2 inner layer after sintering;
top-right corner: surface image to illustrate crack-free surface;
bottom-right corner: section image to illustrate coating thickness [93]

For TiO_2 coating by EPD, the pH value of prepared TiO_2/ethanol suspension was adjusted to 3 as mentioned in the study of Lin et al. [83]. Nanosized TiO_2 powders were deposited on substrate using constant voltage of 10, 20 and 50 V for 60 sec; the surfaces examined for cracks before coating with HA. As shown in Figure 4.19, as the voltage increases, the tendency for crack occurrence increases. Before sintering, when 20 V was used for EPD, samples exhibited crack-free surface (Figure 4.19, main part), the usage of 50 V caused cracks on coatings surface (Figure 4.19, top-right corner). After sintering, cracks on coating surface, for deposition with using 50 V, were more significant (Figure 4.19, bottom-right corner); some spalling and blister at coating surface were observed.

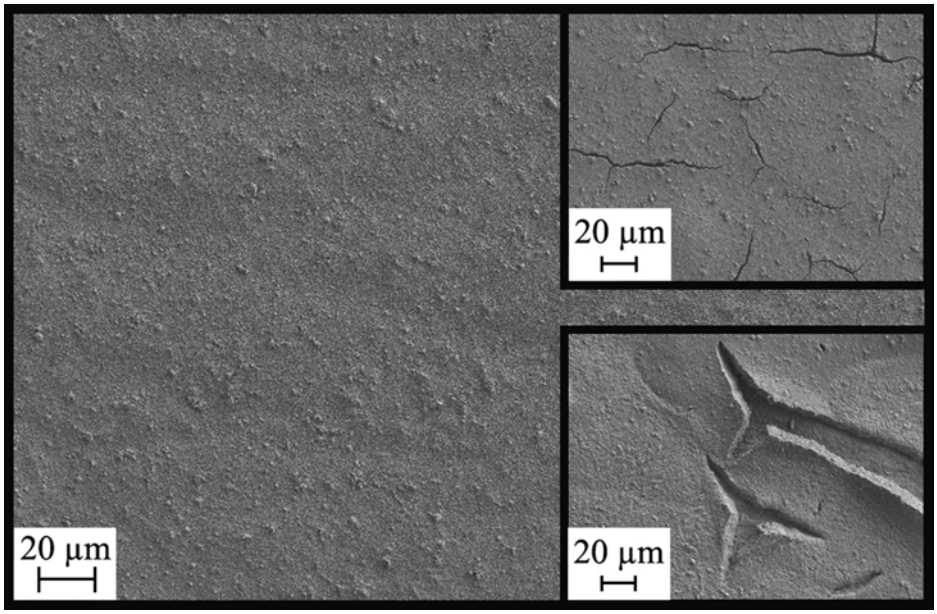

Figure 4.19. SEM micrograph of deposited TiO_2 layer; *main:* TiO_2 deposits using 20 V before sintering; *top-right corner:* TiO_2 deposits using 50 V before sintering; *bottom-right corner:* TiO_2 deposits using 50 V after sintering [93]

In TiO_2 deposition, it was observed that as the voltage increases, the tendency for crack occurrence increases (Figure 4.19). Similar observations were reported in the previous study (in Section 4.2.1) in which uncalcined HA particles were used as coating materials. Also, it was stated that in [42, 51, 66], more adherent and continuous coatings with less cracking can be obtained at lower voltages. It is believed that packing density is responsible for the crack occurrence during drying. In EPD, particle size range increases with applying voltage because apart from the smallest particles, the agglomerated ones can be also deposited on the substrate [66], and this increases the porosity of the deposit [42, 94]. Once a particle comes into contact with the substrate or an already deposited particle, it has no time to move for rearrangement. Therefore, large particles result in the formation of large pores in a particle matrix [14]. In summary, when a lower voltage is applied, a denser packing will occur [14, 42], and the tendency to crack will decrease.

After investigation of crack occurrence on TiO_2 deposits, HA powders were electrophoretically deposited using 200 V for 1 min on TiO_2 coated substrates. For HA coating with TiO_2 inner layer deposited using 20 V, before and after sintering, similar crack-free surfaces as shown in Figure 4.18 (top-right corner) were obtained. For HA

coating on TiO_2 inner layer deposited using 50 V, surface cracks at the TiO_2 layer (Figure 4.19, top-right corner) were filled by HA powders; crack-free surfaces were obtained. However after sintering, some cracks were observed on the HA top layer.

HA coated samples on Ti6Al4V substrate with TiO_2 inner layer deposited using 20 V were analyzed by EDX before and after sintering to illustrate the occurrence of calcium, phosphorus and oxygen on the coating surface, and to determine if any change occurred. EDX spectra and EDX-mapping of sintered specimen are presented in Figure 4.20. It was observed that there were no changes in the HA layer based on the presence of the TiO_2 inner layer.

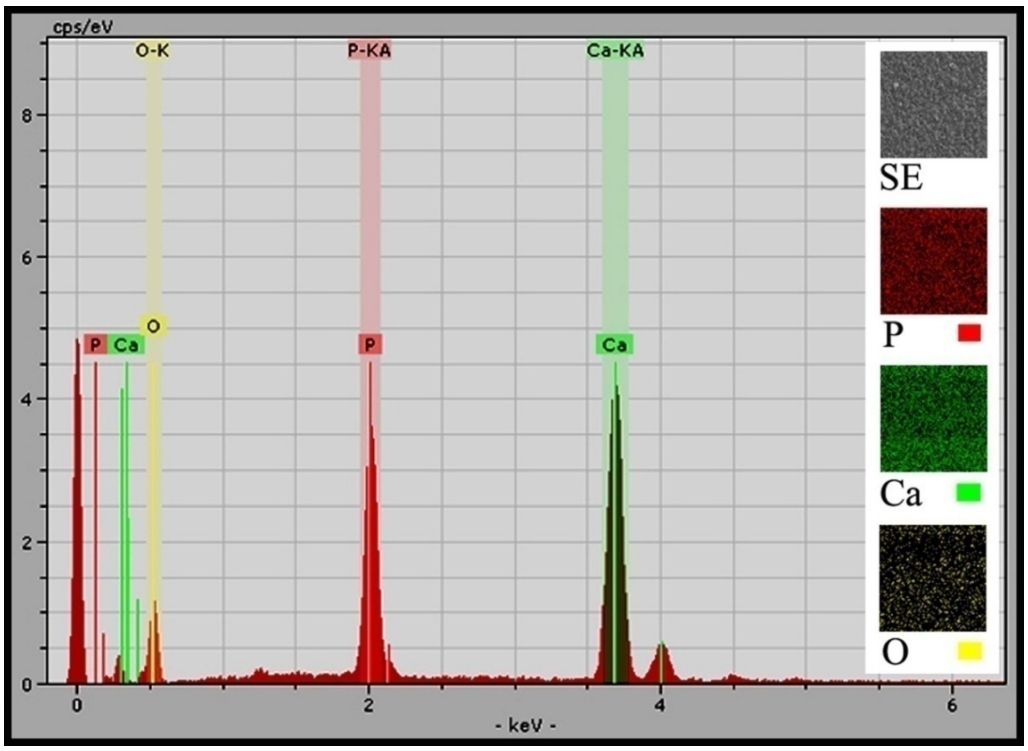

Figure 4.20. EDX analysis to illustrate the elements in top coating layer after sintering (sample: Ti6Al4V substrate, TiO_2 inner layer deposited using 20 V, HA top layer)

After the sintering stage, XRD analyses were performed in order to investigate HA decomposition. The first spectrum at the top in Figure 4.21 is for HA coating; there is no TiO_2 inner layer. On the other spectra, there are TiO_2 inner coating layers deposited using different voltages, 20 and 50 V.

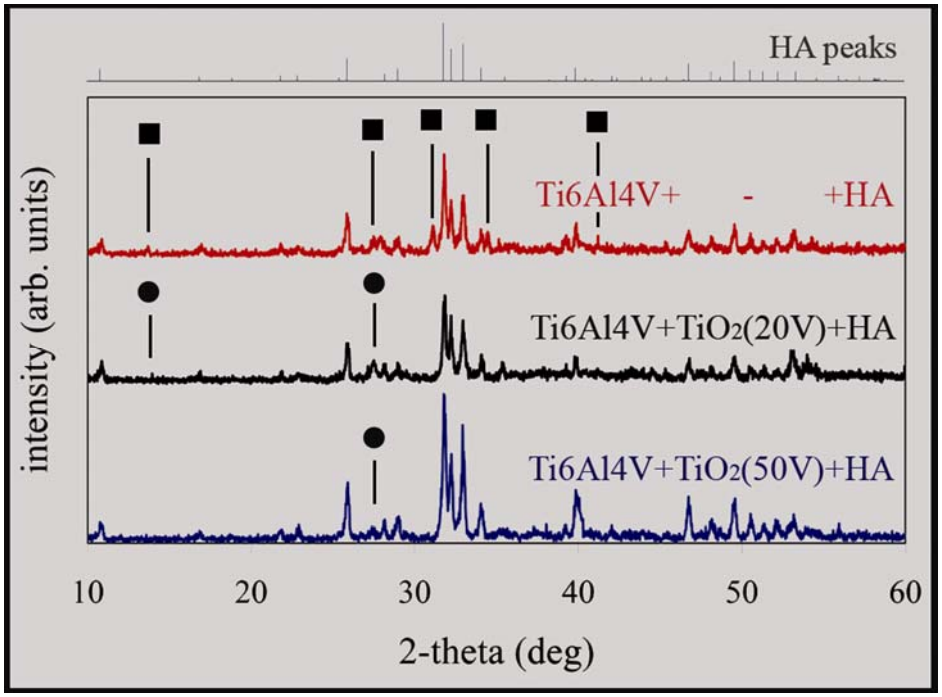

Figure 4.21. XRD spectra of coated samples with and without TiO_2 inner layer after sintering (■ is used for TCP, ● is used for unidentified phase, unsigned peaks are HA)

As shown in the XRD analysis (Figure 4.21) of HA coating on Ti6Al4V substrates, there is some HA decomposition into TCP as mentioned in [51]. The literature reports that the underlying titanium resulted in a partial transformation of HA structure [73, 95], and HA can start to decompose at a temperature as low as 950 °C [12, 72, 96]. The decomposition of HA into TCP induced by Ti begins at lower temperature then TiO_2 [97]. Therefore, the effect of TiO_2 layer on HA decomposition was investigated in the present study, and the comparison of the XRD results (Figure 4.21) demonstrated that the use of TiO_2 inner layer reduced the HA decomposition. The TiO_2 inner coating layer may have acted as a chemical barrier against the release of metal ions from the substrate which prevents HA decomposition as mentioned in [98]. There is no chemical reaction between HA and TiO_2 as can be seen in the XRD and EDX analyses (Figures 4.21 and 4.20, respectively).

Shear test was performed to measure the adhesion strength of HA coatings on Ti6Al4V substrates with and without the TiO_2 inner layer. The data obtained are compiled in Table 4.2 which lists the average adhesion strengths and their standard deviations (in MPa).

Table 4.2. Adhesion strengths of HA coated samples with and without TiO_2 inner layer deposited using different voltages [93]

Samples (substrate + inner layer + HA)	**Shear strength (MPa)**
Ti6Al4V + - + HA	13.8 (s=1.8)
Ti6Al4V + TiO_2 (50 V) + HA	11.9 (s=3.3)
Ti6Al4V + TiO_2 (20 V) + HA	13.1 (s=0.5)
Ti6Al4V + TiO_2 (10 V) + HA	21.0 (s=2.9)

Note. s: standard deviation

The adhesion of the HA coated structure on the Ti6Al4V substrate was quantified by shear strength test following ASTM standard F1044-99 [84] and the studies in References [12, 75, 99]. Although this test and its data analysis methodology are simple and there is an existing standard to follow, careful attention must be paid to the issue of bonding agent (for example, epoxy resin in Figure 3.4) penetration. It is possible that it may penetrate through macropores and partially bond to the substrate, thus invalidating the test result. The presence of epoxy resin at the fracture surface indicates that the measured interfacial stress of the specimen is a false result. Therefore, the shear-fracture surface of the HA coated specimens without TiO_2 inner layer was investigated. It was determined that epoxy resin did not penetrate the fracture surface.

Shear test results on different sets of coatings showed that with the increasing voltage used for the TiO_2 coating, strength decreases (Table 4.2). Increasing voltage used in TiO_2 deposition also increases the tendency for crack formation as shown in Figure 4.19 and decreases the packing density as mentioned above. These cracked and less dense coating layers may result in lower adhesion strength values.

4.2.3. Production of "Calcium Phosphate Based Bioceramics / Titanium Dioxide" Coating Surface on Titanium Substrates

For practical medical applications, such as orthopedic implants, Ca-P coatings with excellent substrate adhesion have been strongly demanded to provide long-time fixation [16]. It is also particularly important for biomaterial applications that such Ca-P coatings

should not be contaminated by toxic materials [17]. In recent years, researches on the bactericidal activity of TiO_2 photocatalyst have been growing [18]. In order to combine the advantages of Ca-P bioceramics and TiO_2, HA/TiO_2 composite coatings [100, 101] have been developed.

In this study, a new method is developed to create a multifunctional surface consisting of Ca-P and TiO_2 on titanium surfaces, where the Ca-P matrix is expected to be responsible for the adsorption of organic substances and bacteria, and where the titanium dioxide is expected to be responsible for decomposition. Chemically synthesized HA nanopowders were produced and used in the EPD as coating material. Samples having cracked surfaces were sintered in air atmosphere, in order to obtain TiO_2 growth (from Ti substrates) inside cracks.

XRD spectra and results of phase identification of synthesized powders at 30 °C for 24 h are presented in Figure 4.4 in which it can be seen that XRD peaks of the dried powders completely match with the HA peaks. Synthetically produced HA nanopowders were used to prepare suspension for EPD, and pH values of the suspension were adjusted to approximately 4 according to zeta potential analysis (Figure 4.12).

HA particles that were produced by acid-base method electrophoretically deposited on Ti substrates. Although cracks are observed at coating surfaces (Figures 4.22 and 4.23a) when the acid-base method is used (as stated by Wei et al [74] and Albayrak et al. [82]), this method has been preferred since the reaction involves no foreign element and the only by-product is water. To obtain formation of TiO_2 on Ti substrates in the crack regions samples deliberately prepared with crack surfaces (Figures 4.22 and 4.23a) were sintered in air atmosphere. As predicted, TiO_2 growth was observed inside the cracks (Figure 4.23b).

XRD spectra and results of phase identification for coating surfaces after sintering stage were presented in Figure 4.24. It revealed that the sintered coating was composed of TiO_2 crystal structure with rutile (ICDD PDF No: 77-441) and β-TCP phases (ICDD PDF No: 9-169). Sintering of the HA coated Ti substrates at 1000 °C for 2 h induced HA decomposition to TCP. Atomic percents of Ca and P were determined as 60 and 40, respectively (Ca/P=1.5) by quantitative EDX analysis.

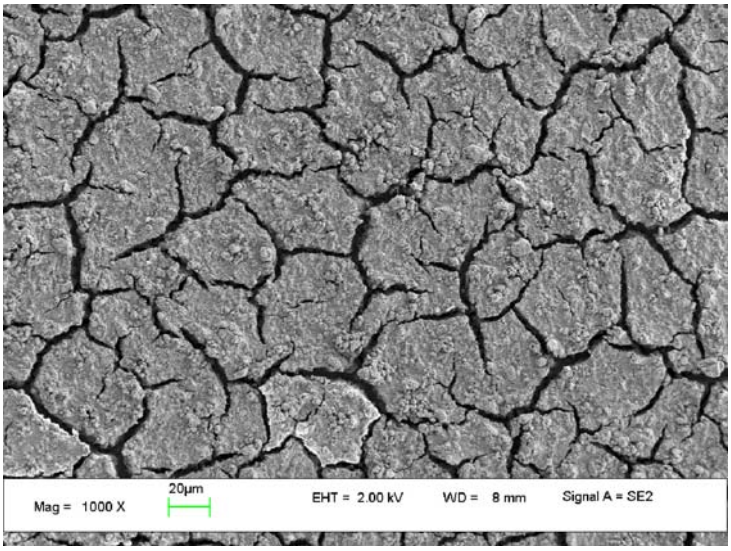

Figure 4.22. SEM images of coating surfaces before sintering stage (uncalcined HA powders)

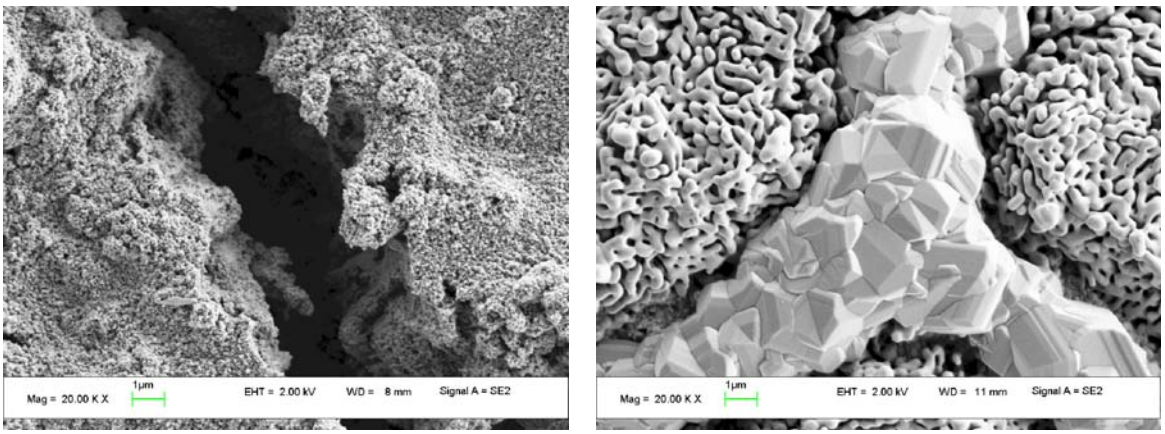

(a) (b)

Figure 4.23. TiO_2 growth inside cracks: (a) before sintering stage, (b) after sintering stage

Compared with HA, TCP has a lower Ca/P ratio, which increases the degradation rate when the ceramic is placed in a biological environment [102-104]. Degradation of implanted ceramics allows bone in-growth and eventual replacement of the artificial material with natural tissue [104].

EDX-mapping (Figure 4.25) of these sintered samples were used to show the presence of Ca, P, Ti and O in coating surface. These elemental scans revealed that Ca and P were determined at surface except cracked regions in which Ti were visualized.

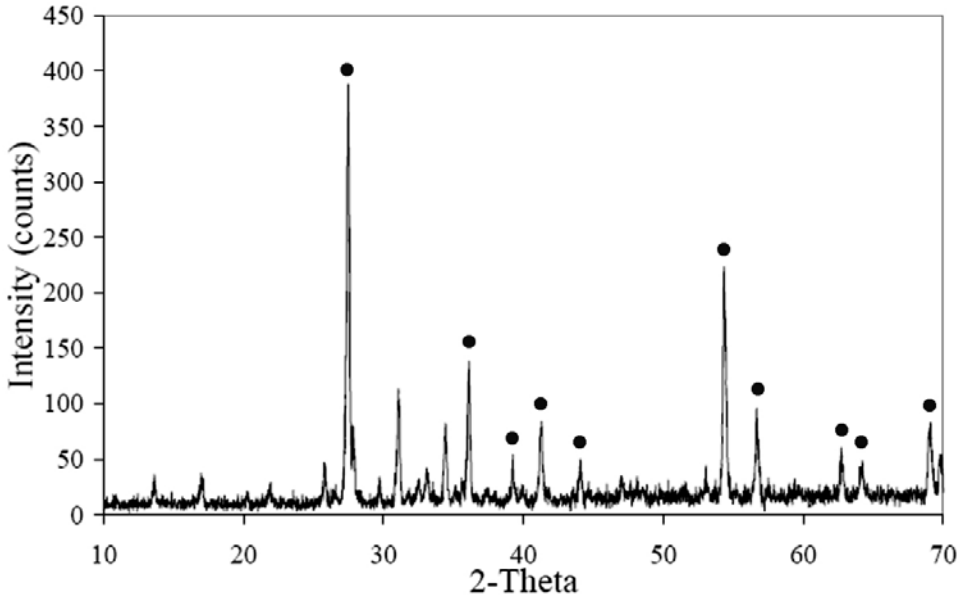

Figure 4.24. XRD spectra of coating surface
(● is used for TiO_2, all other unsigned peaks are TCP)

It is particularly important for biomaterial applications that such Ca-P coatings should not be contaminated by toxic materials [17]. At the present study, coating consisting of Ca-P and TiO_2 were produced on titanium substrate with the expectation of a synergistic effect of the adsorption of the Ca-P and photocatalytic activity of the TiO_2. The bactericidal effect of TiO_2 is the advantage for obtaining antibacterial coating surface.

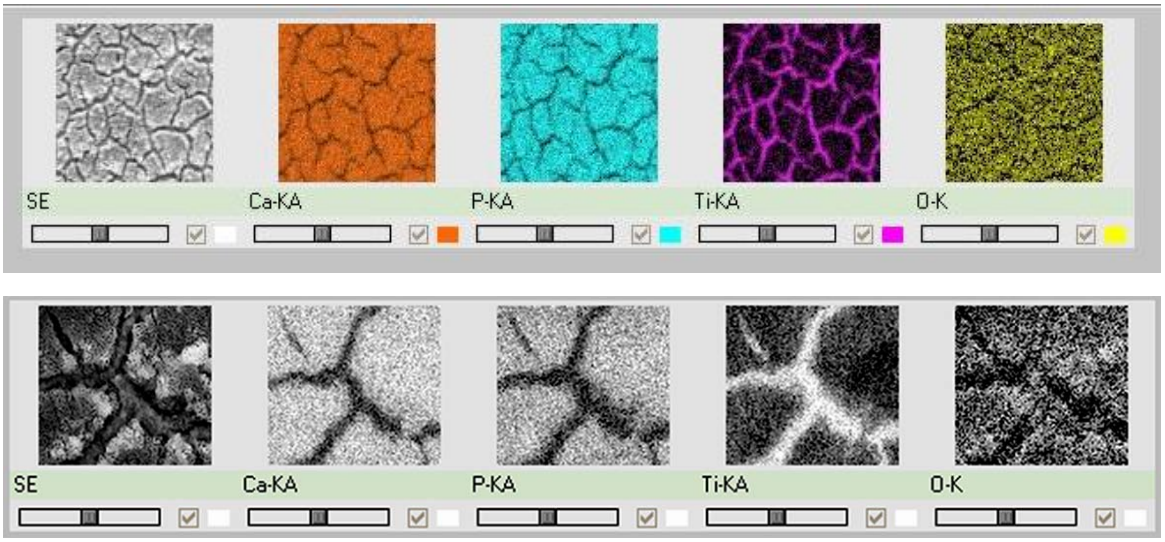

Figure 4.25. EDX-mapping of coating surfaces obtained different magnification

SEM micrograph of Figure 4.26 revealed that, open-pore structure and coalescence between TCP and TiO_2 were obtained. Coalescence of TCP/TiO_2 is expected to increase the adhesion strength of coating.

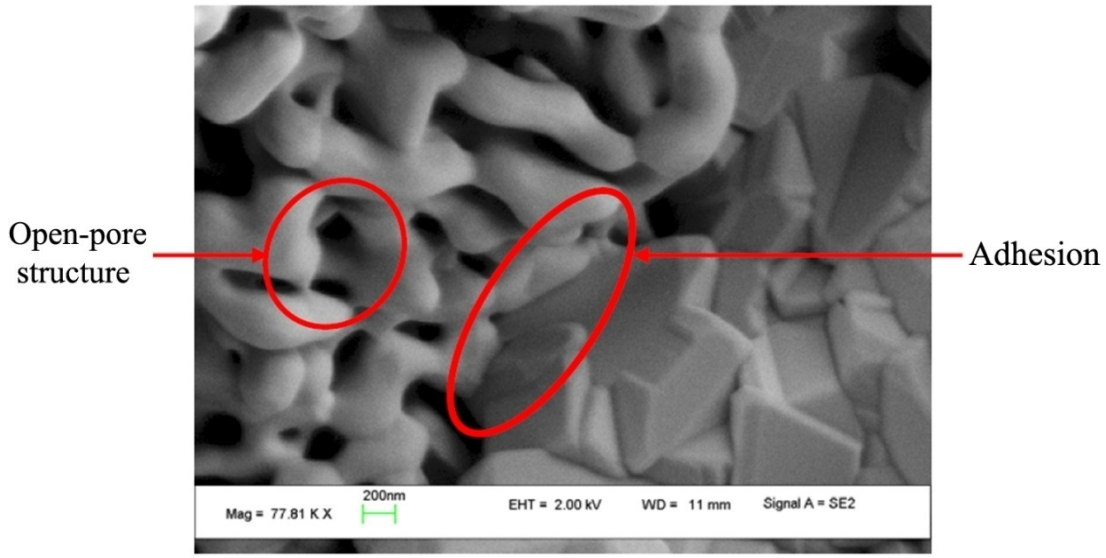

Figure 4.26. Coalescence of TCP and TiO_2 on coating surface

5. CONCLUSIONS

In this study, chemically synthesized (nano sized) and naturally derived (submicron sized) hydroxyapatite (HA) powders were successfully produced and used for coating Ti and Ti6Al4V substrates by using electrophoretic deposition (EPD) method. Experiments were conducted towards preventing crack occurrence and low adhesion strength which are problems frequently encountered in EPD coating. Furthermore, studies were conducted to create coating surfaces consisting of Ca-P and TiO_2. Following conclusions can be drawn from these studies:

- For the nano powders synthesized using different parameters (temperature and time), XRD peaks of all the dried powders completely match with the HA peaks, no other phases are observed. Calcining HA powders at 1000 °C for 1 h induces:
  - High intensity of HA diffraction peaks together with minor TCP peaks for powders synthesized at 30 °C for 24 h.
  - High intensity of HA diffraction peaks together with minor CaO peaks for powders synthesized at 85 °C for 10 min and 24 h.
  - Completely HA peaks, no other phases are present for powders synthesized at 40 °C for 24 h and 48 h.

- Successful production of thermally stable HA powders up to 1200 °C were achieved by chemical synthesis at 40 °C for 24 h, and also by naturally deriving HA from calf femoral bone.

- Synthetic nano sized HA powders present better compaction, and have higher hardness and compression values than naturally derived sub-micron sized HA. For samples sintered at 1200 °C for 2 h, microhardness value is about 640 HV for synthetically produced nano powders, while about 240 HV for naturally produced sub-micron powders.

- HA powders produced by the acid-base method exhibit needle-like shapes (about 120 nm by 40 nm) with an approximate aspect ratio of 3:1. After calcination at 1000 °C

for 1 h, these particles are observed to slightly coarsen and their shapes turn to nodular-like (about 180 nm by 150 nm) with an approximate aspect ratio of 1.2:1.

- The use of uncalcined powders in EPD caused cracks on coating surface, while calcined powders exhibit crack-free surfaces even after sintering stage. The cracking susceptibility depends on the particle shape; the more regular the particle shape becomes (the closer it is to equal-axed), the less is the cracking susceptibility. Obviously, drying shrinkage is minimized by the use of nodular shaped particles that can pack efficiently.

- A dense and homogeneous inner layer is expected to contribute to high adhesion strength between the HA layer and the substrate. Therefore, TiO_2 powders of 32 nm average particle size are deposited on the Ti6Al4V substrate which is followed by the deposition of the calcined HA powders of approximately 150 nm. Adhesion strength of the overall coating was increased with the decreasing voltage value used for TiO_2 deposit (it was observed that crack occurrence increases with increasing voltage in the TiO_2 coating on Ti6Al4V substrate using EPD with different voltages as 10, 20 and 50 V for 1 min), and also HA decomposition was reduced.

- In the current study, a new method is developed to create surface consisting of Ca-P and TiO_2 on Ti substrates. Coatings with cracks were deliberately prepared by using uncalcined HA nano powders. Studies regarding the effect of the coating voltage on the crack formation have revealed that with increasing voltage value crack formation becomes pronounced. Beyond 100 V spalling of the coating occurs which deteriorates the coating. On the other hand, at low coating voltages the crack is found not to be wide enough to allow TiO_2 growth. Therefore, the coating voltage has been set to 50 V. The coating time has been adjusted to be 60 sec because at longer coating times the coating thickness increases such that the growing TiO_2 from the substrate cannot fill the crack completely up to the surface of the coating. In the HA coatings prepared based on these results, the cracks are satisfactorily covered by TiO_2 after sintering.

REFERENCES

1. Hench, L. L., "Biomaterials: A Forecast for the Future", *Biomaterials*, Vol. 19, No. 16, pp. 1419-1423, 1998.

2. Kivrak, N. and A. C. Tas, "Synthesis of Calcium Hydroxyapatite-Tricalcium Phosphate (HA-TCP) Composite Bioceramics Powders and Their Sintering Behavior", *Journal of American Ceramic Society*, Vol. 81, No. 9, pp. 2245-2252, 1998.

3. Park, J. B. and R. S. Lakes, *Biomaterials: An Introduction*, John Wiley & Sons, New York, 1992.

4. Fufita, R., T. Kawasaki and T. Kohgo, "Bone Augmentation Osteogenesis Using Hydroxyapatite and β-Tricalcium Phosphate Blocks", *Journal of Oral and Maxillofacial Surgery*, Vol. 61, pp. 1045-1053, 2003.

5. Kumta, P. N., C. Sfeir, D. Lee, D. Olton and D. Choi, "Nanostructured Calcium Phosphates for Biomedical Applications: Novel Synthesis and Characterization", *Acta Biomaterialia*, Vol. 1, pp. 65-83, 2005.

6. Kweh, S. W. K., K. A. Khor and P. Cheang, "The Production and Characterization of Hydroxyapatite (HA) Powders", *Journal of Materials Processing Technology*, Vol. 89-90, pp. 373-377, 1999.

7. Saeri, M. R., A. Afshar, M. Ghorbani, N. Ehsani and C. C. Sorrell, "The Wet Precipitation Process of Hydroxyapatite", *Materials Letters*, Vol. 57, pp. 4064-4069, 2003.

8. Nagai, H. and Y. Nishimura, *Hydroxyapatite, ceramic material and process for preparing thereof*, United States Patent, Patent No. 4330514, 1980.

9. Garcia-Sanz, F. J., M. B. Mayor, J. L. Arias, J. Pou, B. Leon and M. Perez-Amor, "Hydroxyapatite Coatings: A Comparative Study Between Plasma-Spray and Pulsed Laser Deposition Techniques", *Journal of Materials Science: Materials in Medicine*, Vol. 8, pp. 861-865, 1997.

10. Stoch, A., A. Brozek, G. Kmita, J. Stoch, W. Jastrzebski and A. Rakowska, "Electrophoretic Coating of Hydroxyapatite on Titanium Implants", *Journal of Molecular Structure*, Vol. 596, pp. 191-200, 2001.

11. Yildirim, O. S., B. Aksakal, H. Celik, Y. Vangolu and A. Okur, "An Investigation of the Effects of Hydroxyapatite Coatings on the Fixation Strength of Cortical Screws", *Medical Engineering and Physics*, Vol. 27, pp. 221-228, 2005.

12. Wei, M., A. J. Ruys, B. K. Milthorpe, C. C. Sorrell and J. H. Evans, "Electrophoretic Deposition of Hydroxyapatite Coatings on Metal Substrates: A Nanoparticulate Dual-Coating Approach", *Journal of Sol-Gel Science and Technology*, Vol. 21, pp. 39-48, 2001.

13. Mavis, B. and A. C. Tas, "Dip-Coating of Calcium Hydroxyapatite on Ti-6Al-4V Substrates", *Journal of American Ceramic Society*, Vol. 83, pp. 989-991, 2000.

14. Ma, J., C. Wang and K. W. Peng, "Electrophoretic Deposition of Porous Hydroxyapatite Scaffold", *Biomaterials*, Vol. 24, pp. 3505-3510, 2003.

15. Wang, Z. C., F. Chen, L. M. Huang and C. J. Lin, "Electrophoretic Deposition and Characterization of Nano-Sized Hydroxyapatite Particles", *Journal of Materials Science*, Vol. 40, No. 18, pp. 4955-4957, 2005.

16. Sun, L., K. A. Gross and A. Kucuk, "Material Fundamentals and Clinical Performance of Plasma-Sprayed Hydroxyapatite Coatings: A Review", *Journal of Biomedical Materials Research*, Vol. 58, pp. 570-592, 2001.

17. Inagaki, M. and T. Kameyama, "Effects of Plasma Gas Composition on Bond Strength of Hydroxyapatite/Titanium Composite Coatings Prepared by rf-plasma Spraying", *Journal of the European Ceramic Society*, Vol. 26, pp. 495-499, 2006.

18. Daoud, W. A. and Y. H. Zhang, "Surface Functionalization of Cellulose Fibers with Titanium Dioxide Nanoparticles and Their Combined Bactericidal Activities", *Surface Science*, Vol. 599, pp. 69-75, 2005.

19. Nonami, T. and K. Funakoshi, "Apatite-Coated Titanium Dioxide Photocatalyst for Air Purification", *Catalysis Today*, Vol. 96, pp. 113-118, 2004.

20. Blanchard, C. R., *Biomaterials: Body Parts of the Future*, http://www.swri.org/3pubs/ttoday/fall/implant.htm, 1995.

21. Szycher, M., "Biomaterials", in J. Kline (ed.), *Handbook of Biomedical Engineering*, pp. 441-457, Academic Press, California, 1988.

22. Brunski, J. B., "Metals", in B. D. Ratner, A.S. Hoffman, F. J. Schoen and J. E. Lemons (eds.), *Biomaterials Science: An Introduction to Materials in Medicine*, pp. 137-153, Academic Press, California, 2004.

23. Heness, G. and B. Ben-Nissan, "Innovative Bioceramics", *Materials Forum*, Vol. 27, pp. 104-114, 2004.

24. Katz, J. L., L. L. Latta, S. Singh and H. S. Yoon, "Biomechanics of Orthopedics and Rehabilitation of the Musculoskeletal System", in J. Kline (ed.), *Handbook of Biomedical Engineering*, pp. 459-524, Academic Press, California, 1988.

25. Imam, M. A. and A. C. Fraker, "Titanium Alloys as Implant Materials", in. J. E. Lemons and S. A. Brown (eds.), *Medical Applications of Titanium and Its Alloys: The Material and Biological Issues*, pp. 3-16, ASTM Publication, 1996.

26. Dee, K. C., D. A. Puleo and R. Bizios, *An Introduction to Tissue-Biomaterial Interactions*, John Wiley & Sons, New Jersey, 2002.

27. Thamaraiselvi, T. V. and S. Rajeswari, "Biological Evaluation of Bioceramic Materials - A Review", *Trends in Biomaterials and Artificial Organs*, Vol. 18, No. 1, pp. 9-17, 2004.

28. Best, S. M., A. E. Porter, E. S. Thian and J. Huang, "Bioceramics: Past, Present and for the Future", *Journal of the European Ceramic Society*, Vol. 28, pp. 1319-1327, 2008.

29. Dubok, V. A., "Bioceramics - Yesterday, Today, Tomorrow", *Powder Metallurgy and Metal Ceramics*, Vol. 39, No. 7-8, pp. 381-394, 2000.

30. Hench, L. L. and S. Best, "Ceramics, Glasses, and Glass-ceramics", in A. S. Hoffman, F. J. Schoen, J. E. Lemans and B. D. Ratner (eds.), *Biomaterials Science: An Introduction to Materials in Medicine*, pp. 153-169, Academic Press, California, 2004.

31. Raynaud, S., D. Bernache-Assollant and P. Thomas, "Calcium Phosphate Apatites with Variable Ca/P Atomic Ratio I. Synthesis, Characterization and Thermal Stability of Powders", *Biomaterials*, Vol. 23, pp. 1065-1072, 2002.

32. Tas, A. C., M. Timucin and N. Akkas, "An Investigation of the Chemical Synthesis and High-temperature Sintering Behavior of Calcium Hydroxyapatite (HA) and Tricalcium Phosphate (TCP) Bioceramics", *Journal of Materials Science: Materials in Medicine*, Vol. 8, pp. 91-96, 1997.

33. Wang, H., "Ca/P ratio on the Degradation of Hydroxyapatite in Vitro", *Journal of Biomedical Materials Research: Part A*, Vol. 67A, pp. 599-608, 2003.

34. Hench, L. L. and J. Wilson, "Bioceramics", *MRS Bulletin*, Vol. 9, pp. 62-74, 1991.

35. Ozeki, K., H. Aoki and Y. Fukui, "Photocatalytic Hydroxyapatite/Titanium Dioxide Multilayer Thin Film Deposited onto Glass Using an rf Magnetron Sputtering Technique", *Applied Surface Science*, Vol. 253, pp. 3397-3401, 2007.

36. Wei, M., *Electrophoresis of Hydroxyapatite on Metal Substrates*, Ph.D. Thesis, University of New South Wales, 1997.

37. Goren, S., H. Gokbayrak and S. Altintas, "Production of Hydroxylapatite from Animal Bone", *Key Engineering Materials*, Vol. 264-268, pp. 1949-1952, 2004.

38. Haberko, K., M. M. Bucko, J. Brzezinska-Miecznik, M. Haberko, W. Mozgawa, T. Panz, A. Pyda and J. Zarebski, "Natural Hydroxyapatite: Its Behavior During Heat Treatment", *Journal of the European Ceramic Society*, Vol. 26, pp. 537-542, 2006.

39. Hiller, J. C., T. J. U. Thompson, M. P. Evison, A. T. Chamberlain and T. J. Wess, "Bone Mineral Change during Experimental Heating: An X-ray Scattering Investigation", *Biomaterials*, Vol. 24, pp. 5091-5097, 2003.

40. İpekoglu, M., *Effects of Calcination and Particle Size on the Sintering of Natural Hydroxyapatite*, M.Sc. Thesis, Boğaziçi University, 2004.

41. Ma, J., "Colloidal Characterization and Electrophoretic Deposition of Hydroxyapatite on Titanium Substrate", *Journal of Materials Science: Materials in Medicine*, Vol. 14, pp. 797-801, 2003.

42. Zhitomirsky, I. and L. Gal-Or, "Electrophoretic Deposition of Hydroxyapatite", *Journal of Materials Science: Materials in Medicine*, Vol. 8, pp. 213-219, 1997.

43. Lim, Y. M., Y. J. Park, Y. Yun and Y. K. S. Hwang, "Functionally Graded Ti/HAP Coatings on Ti-6Al-4V Obtained by Chemical Solution Deposition", *Ceramics International*, Vol. 28, pp. 37-41, 2002.

44. Sena, L. A., M. C. Andrade, A. M. Rossi and G. A. Soares, "Hydroxyapatite Deposition by Electrophoresis on Titanium Sheets with Different Surface Finishing", *Journal of Biomedical Materials Research*, Vol. 60, pp. 1-7, 2002.

45. Bharati, S., M. K. Sinha and D. Basu, "Hydroxyapatite Coating by Biomimetic Method on Titanium Alloy Using Concentrated SBF", *Bulletin of Materials Science*, Vol. 28, No. 6, pp. 617-621, 2005.

46. Azom, *Hydroxyapatite: Hydroxyapatite Coatings, an Overview*, http://www.azom.com/details.asp?ArticleID=1405, 2008.

47. Suzdaltsev, E. I. and D. V. Kharitonov, "Methods for the Electrophoretic Shaping of Ceramic Products from Aqueous Slips of Inorganic Materials (a Review)", *Refractories and Industrial Ceramics*, Vol. 45, No. 1, pp. 42-47, 2004.

48. Melvin, M., *Electrophoresis, Analytical Chemistry by Open Learning*, John Wiley & Sons, New York, 1987.

49. Fukada, Y., N. Nagarajan, W. Mekky, Y. Bao, H. S. Kim and P. S. Nicholson, "Electrophoretic Deposition - Mechanisms, Myths and Materials", *Journal of Materials Science*, Vol. 39, pp. 787-801, 2004.

50. Besra, L. and M. Liu, "A Review on Fundamentals and Applications of Electrophoretic Deposition (EPD)", *Progress in Materials Science*, Vol. 52, pp. 1-61, 2007.

51. Wang, C., J. Ma, W. Cheng and R. Zhang, "Thick Hydroxyapatite Coatings by Electrophoretic Deposition", *Materials Letters*, Vol. 57, pp. 99-105, 2002.

52. Datta, S., "Application of Design of Experiment on Electrophoretic Deposition of Glass-Ceramic Coating Materials from an Aqueous Bath", *Bulletin of Materials Science*, Vol. 23, No. 2, pp. 125-129, 2000.

53. Martin-Molina, A., M. Quesada-Perez, F. Galisteo-Gonzales and R. Hidalgo-Alvarez, "Primitive Models and Electrophoresis: An Experimental Study", *Colloids and Surfaces A: Physicochemical and Engineering Aspects*, Vol. 222, pp. 155-164, 2003.

54. *Chem 1909 Lecture Notes: Colloids and Surface Chemistry*, University of Sydney, http://notes.chem.usyd.edu.au/course/fellows/CHEM1909/Colloids.pdf, 2008.

55. Windes, W. E., J. Zimmerman and I. E. Reimanis, "Electrophoretic Deposition Applied to Thick Metal-ceramic Coatings", *Surface & Coatings Technology*, Vol. 157, pp. 267-273, 2002.

56. Shaw, D. J., *Introduction to Colloid & Surface Chemistry*, Reed Educational and Professional Publishing, New York, 1992.

57. Pitts, M. M., *Fouling Mitigation in Aqueous Systems using Electrochemical Water Treatment*, http://www.zetacorp.com/fouling_mitigation.shtml, 2008.

58. Colloidal Dynamics, *Introducing the Zeta Probe*, http://www.colloidal-dynamics.com/applications.htm, 2002.

59. Colloidal Dynamics, *Preparing a Suspension from a Powder*, http://www.colloidal-dynamics.com/techniques.htm, 1999.

60. Azom, *Electrophoresis: Electrophoretic Deposition as Coating Technique*, http://www .azom.com/details.asp?ArticleID=1550, 2008.

61. Winters, T. A., *Notes of the ANS506: Electrophoresis Lecture, Southern Illinois University*, http://www.siu.edu/~tw3a/506eph.htm, 2008.

62. Van Der Biest, O., S. Put, G. Anne and J. Vleugels, "Electrophoretic Deposition for Coating and Free Standing Objects", *Journal of Materials Science*, Vol. 39, pp. 779-785, 2004.

63. Buckley, N. E., *Bio-451 Molecular Biology Techniques - Lecture 4: Electrophoresis, California State Polytechnic University*, http://www.csupomona.edu/~nebuckley/Courses/Bio451/Lectures/Bio451Lecture4.htm, 2008.

64. Chaim, R., I. Zhitomirsky, L. Gal-Or and H. Bestgen, "Electrochemical Al_2O_3–ZrO_2 Composite Coatings on Non-oxide Ceramic Substrates", *Journal of Materials Science*, Vol. 32, pp. 389-400, 1997.

65. Maca, K., H. Hadraba and J. Cihlar, "Electrophoretic Deposition of Alumina and Zirconia I. Single-component Systems", *Ceramics International*, Vol. 30, pp. 843-852, 2004.

66. Mondragon-Cortez, P. and G. Vargas-Gutierrez, "Electrophoretic Deposition of Hydroxyapatite Submicron Particles at High Voltages", *Materials Letters*, Vol. 58, pp. 1336-1339, 2004.

67. Ozawa, N., Y. Ideta, K. Shimizu and T. Yao, "Development of a Bioactive Alumina-Based Composite by Electrophoretic Deposition", *Key Engineering Materials*, Vol. 240-242, pp. 67-70, 2003.

68. Nie, X., A. Leyland and A. Matthews, "Deposition of Layered Bioceramic HAP/TiO_2 Coatings on Titanium Alloys Using a Hybrid Technique of Micro-Arc Oxidation and Electrophoresis", *Surface & Coatings Technology*, Vol. 125, pp. 407-414, 2000.

69. Nakahira, A., F. Nishimura, S. Kato, M. Iwata and S. Takeda, "Green Fabrication of Porous Ceramics Using an Aqueous Electrophoretic Deposition Process", *Journal of American Ceramic Society*, Vol. 86, pp. 1230-1232, 2003.

70. Zhitomirsky, I., "Electrophoretic Hydroxyapatite Coatings and Fibers", *Materials Letters*, Vol. 42, pp. 262-271, 2000.

71. Van Der Biest, O., *Electrophoretic deposition (EPD)*, http://www.mtm.kuleuven.ac.be/Research/C2/EPD.htm, 2008.

72. Sridhar, T. M., U. Kamachi Mudali and M. Subbaiyan, "Sintering Atmosphere and Temperature Effects on Hydroxyapatite Coated Type 316L Stainless Steel", *Corrosion Science*, Vol. 45, pp. 2337-2359, 2003.

73. Ducheyne, P., S. Radin and M. Heughebaert, "Calcium Phosphate Ceramic Coatings on Porous Titanium: Effect of Structure and Composition on Electrophoretic Deposition, Vacuum Sintering and in Vitro Dissolution", *Biomaterials*, Vol. 11, pp. 244-254, 1990.

74. Wei, M., A. J. Ruys, B. K. Milthorpe and C. C. Sorrell, "Precipitation of Hydroxyapatite Nanoparticles: Effects of Precipitation Method on Electrophoretic Deposition", *Journal of Materials Science: Materials in Medicine*, Vol. 16, pp. 319-324, 2005.

75. Wei, M., A. J. Ruys, M. V. Swain, S. H. Kim, B. K. Milthorpe and C. C. Sorrell, "Interfacial Bond Strength of Electrophoretically Deposited Hydroxyapatite Coatings on Metals", *Journal of Materials Science: Materials in Medicine*, Vol. 10, pp. 401-409, 1999.

76. Sridhar, T. M., U. Kamachi Mudali and M. Subbaiyan, "Preparation and Characterization of Electrophoretically Deposited Hydroxyapatite Coatings on Type 316L Stainless Steel", *Corrosion Science*, Vol. 45, pp. 237-252, 2003.

77. Xiao, X. F. and R. F. Liu, "Effect of Suspension Stability on Electrophoretic Deposition of Hydroxyapatite Coatings", *Materials Letters*, Vol. 60, No. 21-22, pp. 2627-2632, 2006.

78. Iwasaki, K., "Production of a Functionally Graded Artificial Tooth Root by Unique Sequence of Processes", *Materials Research Innovations*, Vol. 1, pp. 180-187, 1997.

79. Toop Kumar, R. and M. Wang, "Functionally Graded Bioactive Coatings of Hydroxyapatite / Titanium Oxide Composite System", *Materials Letters*, Vol. 55, pp. 133-137, 2002.

80. Hadraba, H., K. Maca and J. Cihla, "Electrophoretic Deposition of Alumina and Zirconia II: Two-component Systems", *Ceramics International*, Vol. 30, pp. 853-863, 2004.

81. Ipekoglu, M. and S. Altintas, "Sintering of Naturally Hydroxyapatite with Boron Oxide Addition", *12th International Conference on Composites/Nano Engineering Proceedings*, Tenerife - Spain, 01-06 August 2005, CD-ROM, 2005.

82. Albayrak, O., C. Oncel, M. Tefek and S. Altintas, "Effects of Calcination on Electrophoretic Deposition of Naturally Derived and Chemically Synthesized Hydroxyapatite", *Reviews on Advanced Materials Science*, Vol. 15, pp. 10-15, 2007.

83. Lin, C. K., T. J. Yang, Y. C. Feng, T. T. Tsung and C. Y. Su, "Characterization of Electrophoretically Deposited Nanocrystalline Titanium Dioxide Films", *Surface & Coatings Technology*, Vol. 200, pp. 3184-3189, 2006.

84. ASTM Standard F1044-99, Standard Test Method for Shear Testing of Calcium Phosphate Coating and Metallic Coatings, 1999.

85. Koutsopoulus, S., "Synthesis and Characterization of Hydroxyapatite Crystals. A Review Study on the Analytical Methods", *Journal of Biomedical Materials Research*, Vol. 62, No. 4, pp. 600-612, 2002.

86. Afshar, A., M. Ghorbani, N. Ehsani, M. R. Saeri and C. C. Sorrell, "Some Important Factors in Wet Precipitation Process of Hydroxyapatite", *Materials and Design*, Vol. 24, pp. 197-202, 2003.

87. Albayrak, O., G. Cayli, C. Oncel, S. Isci and S. Altintas, "Effects of Process Temperature and Time on the Synthesis of Nanosized Hydroxyapatite", *13th International Metallurgy & Materials Congress, Congress e-Book*, Istanbul, 09-12 November 2006, pp. 718-724, 2006.

88. Rapacz-Kmita, A., C. Paluszkiewicz, A. Slosarczyk and Z. Paszkiewicz, "FTIR and XRD Investigations on the Thermal Stability of Hydroxyapatite During Hot Pressing and Pressureless Sintering Processes", *Journal of Molecular Structure*, Vol. 744-747, pp. 653-656, 2005.

89. Mahabole, M. P., R. C. Aiyer, C. V. Ramakrishna, B. Sreedhar and R. S. Khairnar, "Synthesis, Characterization and Gas Sensing Property of Hydroxyapatite Ceramic", *Bulletin of Materials Science*, Vol. 28, No. 6, pp. 535-545, 2005.

90. Liao, C. J., F. H. Lin, K. S. Chen and J. S. Sun, "Thermal Decomposition and Reconstitution of Hydroxyapatite in Air Atmosphere", *Biomaterials*, Vol. 20, pp. 1807-1813, 1999.

91. Albayrak, O., N. Mahmutyazicioglu, M. Ipekoglu, O. El-Atwani and S. Altintas, "Densification and Decomposition Behavior of Isostatically Pressed and Sintered Hydroxyapatite Powders of Nano and Submicron Sizes", *Proceedings of the 10th International Conference of the European Ceramic Society*, Berlin, 17-21 June 2007, pp. 931-935, 2008.

92. Albayrak, O., M. Ipekoglu, C. Oncel and S. Altintas, "Naturally Derived and Synthesized Hydroxyapatite Coating on Titanium Substrates by Electrophoretic Deposition Method", *13th International Metallurgy & Materials Congress, Congress e-Book*, Istanbul, 09-12 November 2006, pp. 480-486, 2006.

93. Albayrak, O., O. El-Atwani and S. Altintas, "Hydroxyapatite Coating on Titanium Substrate by Electrophoretic Deposition Method: Effects of Titanium Dioxide Inner Layer on Adhesion Strength and Hydroxyapatite Decomposition", *Surface & Coatings Technology*, Vol. 202, pp. 2482-2487, 2008.

94. Powers, R. W., "Ceramic Aspects of Forming Beta-Alumina by Electrophoretic Deposition", *American Ceramic Society Bulletin*, Vol. 65, pp. 1270-1277, 1986.

95. Weng, J., X. Liu, X. Zhang and X. Ji, "Thermal Decomposition of Hydroxyapatite Structure Induced by Titanium and its Dioxide", *Journal of Materials Science Letters*, Vol. 13, pp. 159-161, 1994.

96. Ducheyne, P., W. V. Raemdonch, J. C. Heughebaert and M. Heughebaert, "Structural Analysis of Hydroxyapatite Coatings on Titanium", *Biomaterials*, Vol. 7, pp. 97-103, 1986.

97. Manjubala, I. and T. S. Sampath Kumar, "Effect of TiO_2-Ag_2O Additives on the Formation of Calcium Phosphate Based Functionally Graded Bioceramics", *Biomaterials*, Vol. 21, pp. 1995-2002, 2000.

98. Kurzweg, H., R. B. Heimann, T. Troczynski and M. L. Wayman, "Development of Plasma-sprayed Bioceramic Coatings with Bond Coats Based on Titania and Zirconia", *Biomaterials*, Vol. 19, pp. 1507-1511, 1998.

99. Ma, J., C. H. Liang, L. B. Kong and C. Wang, "Colloidal Characterization and Electrophoretic Deposition of Hydroxyapatite on Ti Substrate", *Journal of Materials Science: Materials in Medicine*, Vol. 14, pp. 797-801, 2003.

100. Xiao, X. F. and Y. Z. Zheng, "Characterization of Hydroxyapatite/Titania Composite Coatings Codeposited by a Hydrothermal-Electrochemical Method on Titanium", *Surface & Coatings Technology*, Vol. 200, pp. 4406-4413, 2006.

101. Li, H. and P. Cheang, "Titanium Dioxide Reinforced Hydroxyapatite Coatings Deposited by High Velocity Oxy-fuel (HVOF) Spray", *Biomaterials*, Vol. 23, pp. 85-91, 2002.

102. Oh, K. S., F. Caroff, R. Famery, M. F. Sigot-Luizard and P. Boch, "Preparation of TCP-TiO_2 Biocomposites and Study of Their Cytocompatibility", *Journal of the European Ceramic Society*, Vol. 18, pp. 1931-1937, 1998.

103. Caroff, F., K. S. Oh, R. Famery and P. Boch, "Sintering of TCP-TiO_2 Biocomposites: Influence of Secondary Phases", *Biomaterials*, Vol. 19, pp. 1451-1454, 1998.

104. Seeley, Z., A. Bandyopadhyay and S. Bose, "Tricalcium Phosphate Based Resorbable Ceramics: Influence of NaF and CaO Addition", *Materials Science and Engineering C*, Vol. 28, No. 1, pp. 11-17, 2007.